U-Th Dating of Zircons from a Holocene Volcanic Eruption (Dayingshan Volcano, Tengchong Volcanic Field): Insights into Magma Chamber Storage

by

Ross Thomas Tucker

A thesis submitted to the Graduate Faculty of
Auburn University
in partial fulfillment of
requirements for the Degree of
Master of Science

Auburn, Alabama
August 6, 2011

Approved by

Haibo Zou, Chair, Assistant Professor of Geology
Mark G. Steltenpohl, Professor of Geology
Willis E. Hames, Professor of Geology

Abstract

The Tengchong volcanic field is located along the southeastern margin of the Tibetan Plateau and has shown active volcanism throughout the Cenozoic. Only three volcanoes, however, have erupted more recently in the Holocene. The source of this volcanism is poorly understood due to several unique eruptive stages. The Holocene volcanic rocks derive from a potassic melt with high SiO_2 content (62 wt. %) and an abundance of zircon grains. Zircon is renowned for its important role in geochronology and crustal evolution studies. This research utilizes U-Th dating methods and secondary ion mass spectrometry to date zircons from the Dayingshan volcano, which can be used to provide constraints on magma chamber storage time.

Whole-rock major and trace element analyses from Dayingshan indicate high Zr concentrations and a calc-alkaline suite. Trace elements plotted on a spider diagram reflect magma generation involving hydrous fluids in the mantle overlying a downgoing lithospheric slab. Measured zircon cores yielded an age of 87.5 ± 6.5 ka, while zircon rims yielded an age of 58 ± 13 ka. These different ages represent two separate magmatic events. The older age population is interpreted as antecrysts remobilized from an earlier magmatic episode. The calculated magma chamber storage time for the most recent Dayingshan eruption is 48 ka. Trace element and isotopic data suggest hydrous melting of a stagnant slab from earlier subduction as the likely cause for the continental crust signatures of the magma.

Acknowledgments

Funding for this research was graciously provided by Haibo Zou via a National Science Foundation (NSF) grant (EAR-0917651). Funding for travel was provided by the Auburn University College of Science and Mathematics. Axel Schmitt provided guidance and instruction on the operation of SIMS. Thanks are owed to him, Kevin McKeegan, Mark Harrison, and all others who participated in the NSF National Ion Microprobe Student Workshop hosted by UCLA. Thanks are owed to Clint Barineau and Columbus State University for providing the facilities and equipment for zircon extraction, as well as valuable instruction on the zircon extraction process. Special thanks are owed to Haibo Zou for providing funding, materials, valuable insights into the field area, assistance in sample preparation, and instruction on the operation of SIMS. Thanks are also owed to thesis committee members Mark Steltenpohl and Bill Hames for their valuable suggestions and comments that improved the quality of this thesis. Finally, thanks are owed to my parents, Tom and Becky Tucker, for providing every kind of support throughout my undergraduate and graduate studies.

Table of Contents

List of Tables

List of Figures

INTRODUCTION

Volcanism in the Tibetan Plateau has been occurring throughout the Cenozoic since the development of the Himalayas. The Tengchong volcanic field (TVF) (Fig. 1) is located in the southeastern portion of the Tibetan Plateau (24°40'-25°30'N, 98°15'-98°45'E), and has recorded active volcanism from ~ 5 Ma to ~10 ka (Zhu et al., 1983; Zou et al., 2010). Maanshan, Dayingshan, and Heikongshan are the three most recently active volcanoes in the TVF, each with recorded Holocene (<10 ka) eruptions. These volcanoes are considered dormant, as they still have eruptive potential. The volcanism is derived from a potassic melt, and is post-collisional, as the continental collision that developed the Himalayas initiated much earlier (~65 Ma). There are numerous hot springs in the area, indicating active geothermal fields that show potential for volcanic eruptions (Zhiquan, 2005). The origin of the potassic volcanism is ambiguous, and rocks appropriate for U-Th dating are rare in the Tibetan Plateau.

Young, Holocene volcanic rocks from the TVF contain zircon crystals suitable for U-Th disequilibrium studies (Zou et al., 2010). Zircon analysis is a critical tool in the fields of geochemistry and geochronology due to its ability to incorporate and retain elemental and isotopic information. This retained information is crucial for understanding the nature, origin and age of a particular rock. Of particular interest is the ability of zircon to incorporate radioactive Uranium isotopes into its crystal structure. The incorporation of this isotope allows geologists to determine an absolute age of a rock sample through radiometric dating, which is done by measuring the amount of parent

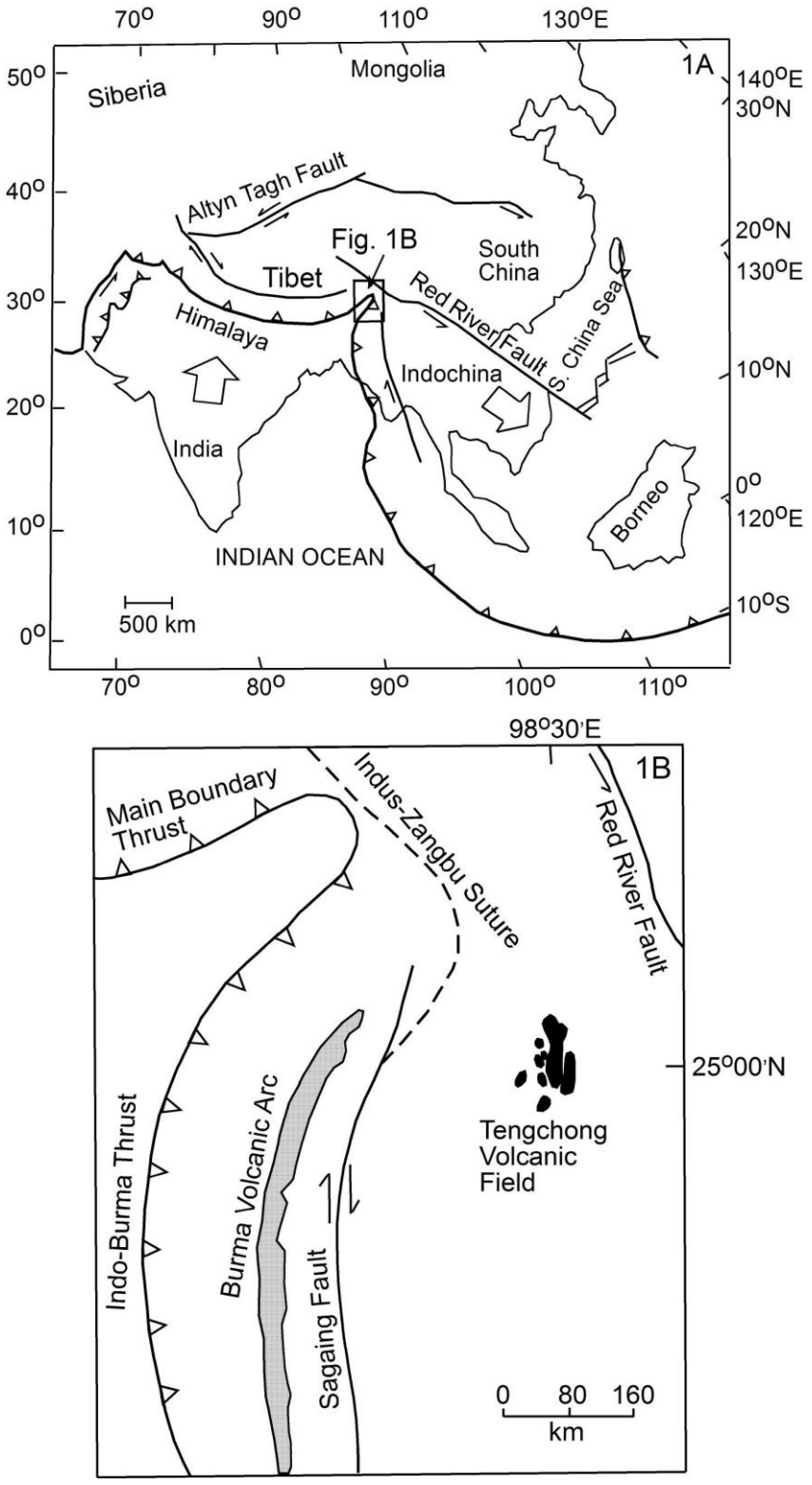

Fig. 1. Location map of the Tengchong volcanic field in SE China. TVF lies in a N-S trending fault zone between the Sagaing and Red River faults, and lies ~200 km from the subduction-related Burma volcanic arc (After Zou et al., 2009).

isotopes (U) in relation to the amount of daughter isotopes (Pb or Th) into which the parent decays. While zircon is most widely known for its uses in dating ancient rocks by the ^{238}U-^{206}Pb method, it is also becoming an essential tool in Quaternary geochronology through the ^{238}U-^{230}Th method. This is because zircons are enriched in U and have a large spread in U/Th ratios, and allow for the recording of the pre-eruptive history of a magma up to 350 ka. This is especially useful for determining the storage time of magma within a magma chamber. With the aid of micrometer-scale spatial resolution and high sensitivity provided by secondary ion mass spectrometry (SIMS), a radiometric dating technique that measures the composition of solid materials, individual crystallization events can be recorded from analysis of zircon crystals.

OBJECTIVES

This research attempts to better constrain magma chamber storage time prior to eruption by analysis of samples from the Dayingshan volcano in the Tengchong volcanic field. Of the three recently active volcanoes, Dayingshan was chosen because it has not been previously studied in this regard and has a rich abundance of zircon. Better constraints can be put on magma storage time and magma source generation by zircon and whole-rock analysis. Studies regarding magma storage time are relatively new to the field of geochronology. This research will also demonstrate the capabilities of SIMS dating techniques on Quaternary samples.

The objectives of this study are as follows: (1) to determine the age(s) of zircon crystallization events from Dayingshan volcanic rocks using zircon U-Th dating methods and SIMS; (2) to utilize this data to determine how long magma is stored in the magma chamber before an eruption in this unique volcanic environment; and (3) to potentially determine the source of the volcanism through whole-rock major and trace element analysis.

BACKGROUND

Geologic Setting

The formation of the southwestern region of China is controversial in large part due to its structural complexities. Fan (1978) separated southwestern China into five major tectonic units and briefly summarized a likely history of tectonic evolution. The major tectonic events are a collision between the Chinese (Amurian) and Eurasian plates in the Late Triassic, a collisional event between the Tibetan block (Cimmerian terranes?) and Chinese plate, and a final collision between the Indian and Eurasian plates in the Late Cretaceous. Fan (1978) theorized that the Quaternary volcanics in Tengchong likely represent the easternmost edge of the Indian plate; however, more recent geophysical and seismic data (Wang & Long, 1998; Lei et al., 2009) indicate Indian plate subduction does not reach this far East. Possible rotation and extrusion due to the ongoing collision further complicates the heavily faulted region (Tapponnier et al., 1982).

The Tengchong volcanic field is located along the southeastern margin of the Tibetan plateau in the Yunnan province of China. The field is in close proximity to the border of China and Burma, and sits ~450 km from the Indian plate. The field lies in a structurally complex area due to several faults and suture zones that run through and intersect in the area. The Sagaing dextral fault, Myitkyina suture zone, and Burma gneissic belt lie west of the field, while the Gaoligong metamorphic belt and Red River fault zone lie to the east. This has created a N-S fault zone in which the field is situated.

Most of these faults formed as a result of the continental collision between India and Asia. Further to the West is the Burma volcanic arc, which is almost certainly a continental arc developed by shallow continental subduction and melting of the Indo-Australian plate. Volcanism has also been active since the late Tertiary, beginning long after the collision initiated between the Indo-Australian and Eurasian plate (~65 Ma). The field is unique in that it is the only active volcanic zone in the region, as recent geothermal studies suggest that a magmatic reservoir is still present beneath the field (Bai et al., 2002).

Older periods of volcanism are evident in the northern and southern parts of the field, while more recent eruptions have migrated to the central part (Wang, F. et al., 2006). Mu et al. (1987), Ji (1998), and Li et al. (2000) divide eruptions in the area into four major stages: late Miocene-Pliocene basalt and olivine-basalt volcanic rocks (5.5-4.0 and 3.8-0.9 Ma), Pleistocene andesites and dacites (0.8-0.1 Ma), and late Pleistocene-Holocene basalts and basaltic andesites (0.1-0.01 Ma). Table 1 lists these stages and some important characteristics of each. While the field is composed of dominantly basaltic rock, more andesitic rock types are associated with the three youngest volcanoes. Rocks associated with this recent volcanism also contain high abundances of potassium. Wang, Y. et al. (2006) reported a 1.5 to 3.65% increase in K_2O content from the Pliocene to Holocene. Volcanic rocks in the area typically contain high abundances of Al_2O_3 and K_2O and low abundances of TiO_2 and light rare earth elements (LREE) (Wang, Y. et al., 2006). The field's location in a N-S trending fault zone has led to the eastern and western parts of the area being uplifted while the central region has been depressed, creating

Table 1
The four stages of Tengchong volcanism and some characteristics. Distribution data is from Zhu et al. (1983). With the exception of stage 3, there is an increasing trend in K_2O and SiO_2 content through time (Zhu et al., 1983). Ages were determined based on unpublished K-Ar dates by Zhu et al. (1983).

Stage of Volcanism	Age	Dominant rock type	Distribution within field
1	late Miocene-Pliocene	basalt	southeast
	(5.5 - 4 Ma)		
2	late Pliocene-Pleistocene	olivine basalt	north and south
	(3.8-0.9 Ma)		
3	Pleistocene	andesite/dacite	north and southwest
	(0.8-0.1 Ma)		
4	late Pleistocene-Holocene	basalt/basaltic andesite	north and west
	(0.1-0.01 Ma)		

elevation differences of more than 500 m (Wang, Y. et al., 2006). Total crustal thickness in the region is 40-50 km (Zhu et al., 1983).

The formation of the three most recently active volcanoes, Heikongshan, Dayingshan, and Maanshan, is poorly understood. Some believe the melts contain a continental crust component, and are thus generated from subduction and/or wall rock assimilation (Mu et al., 1987; Zhu et al., 1983). Others interpret recent volcanism to be the result of a heterogenous mantle source that incorporates no crustal material at all (Cong et al., 1994). Wang, F. et al. (2006) suggest that both of these sources are likely responsible for generating the lavas. It is probable that there are several different factors contributing to the melt generation and periodic volcanism. Figure 2 is a diagram showing the distribution and relative ages of the three most recently active volcanoes and surrounding rocks.

This study focuses on Dayingshan volcano, the largest of the three active volcanoes in the Tengchong volcanic field. Several episodes of erupted lavas and a large scoria cone make up the volcano, with the most recent rocks consisting of vesicular basaltic andesite. The mineral constituents of the rock are plagioclase and olivine phenocrysts (~10-15%) in a matrix consisting mostly of plagioclase, olivine, augite, and volcanic glass (Fig. 3). A younger lava cone with a lava pool has developed and currently sits beside the primary cone (Wei et al., 2002). Figure 4 shows the distribution of the depositional units erupted from Dayingshan. Rock samples from Dayingshan can be dated due to a relative abundance of the mineral zircon.

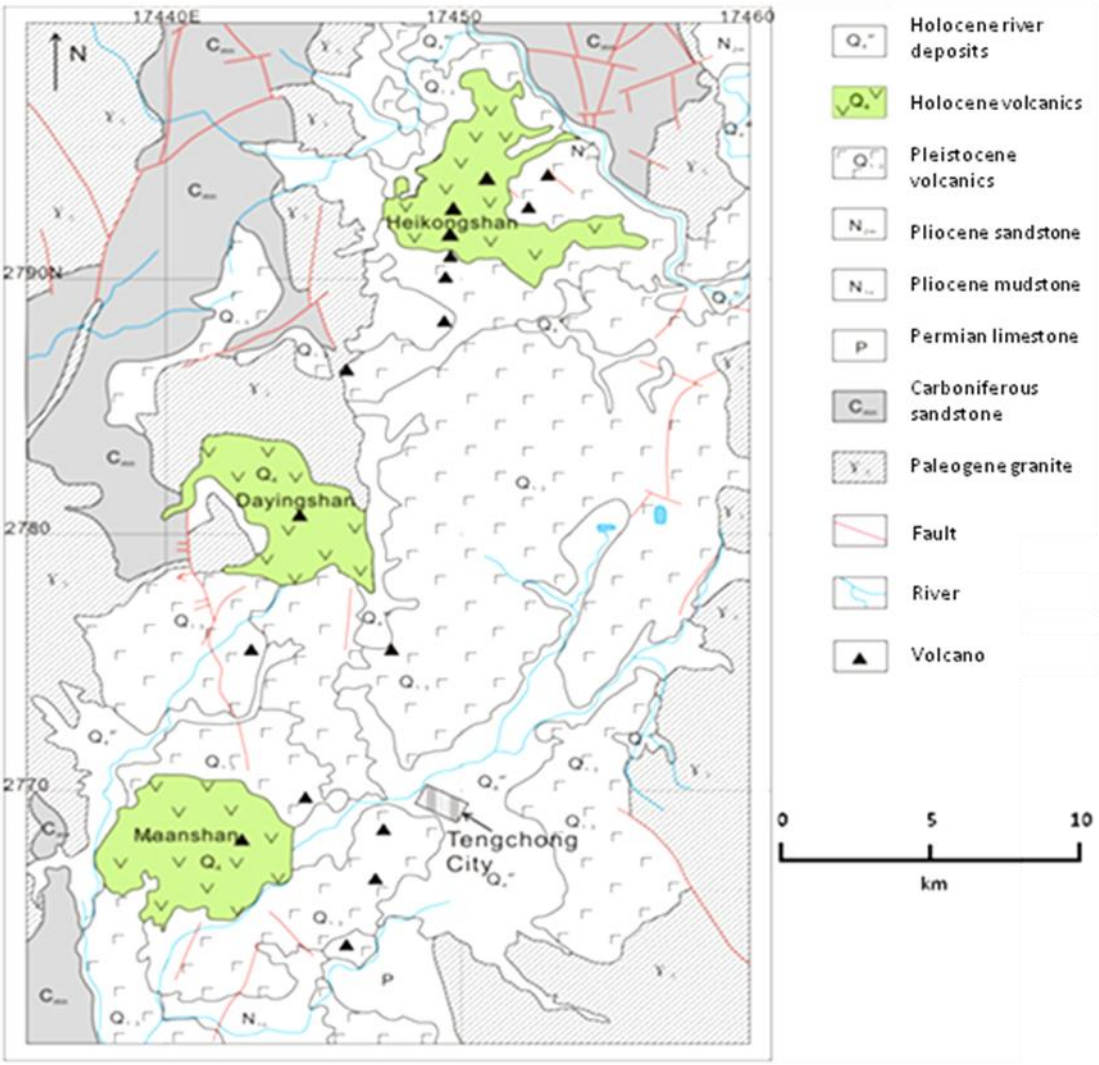

Fig. 2. Distribution and relative ages of the three most recently active volcanoes and surrounding rocks. Most volcanoes represented are small cinder cones (Modified from Zou et al., 2009).

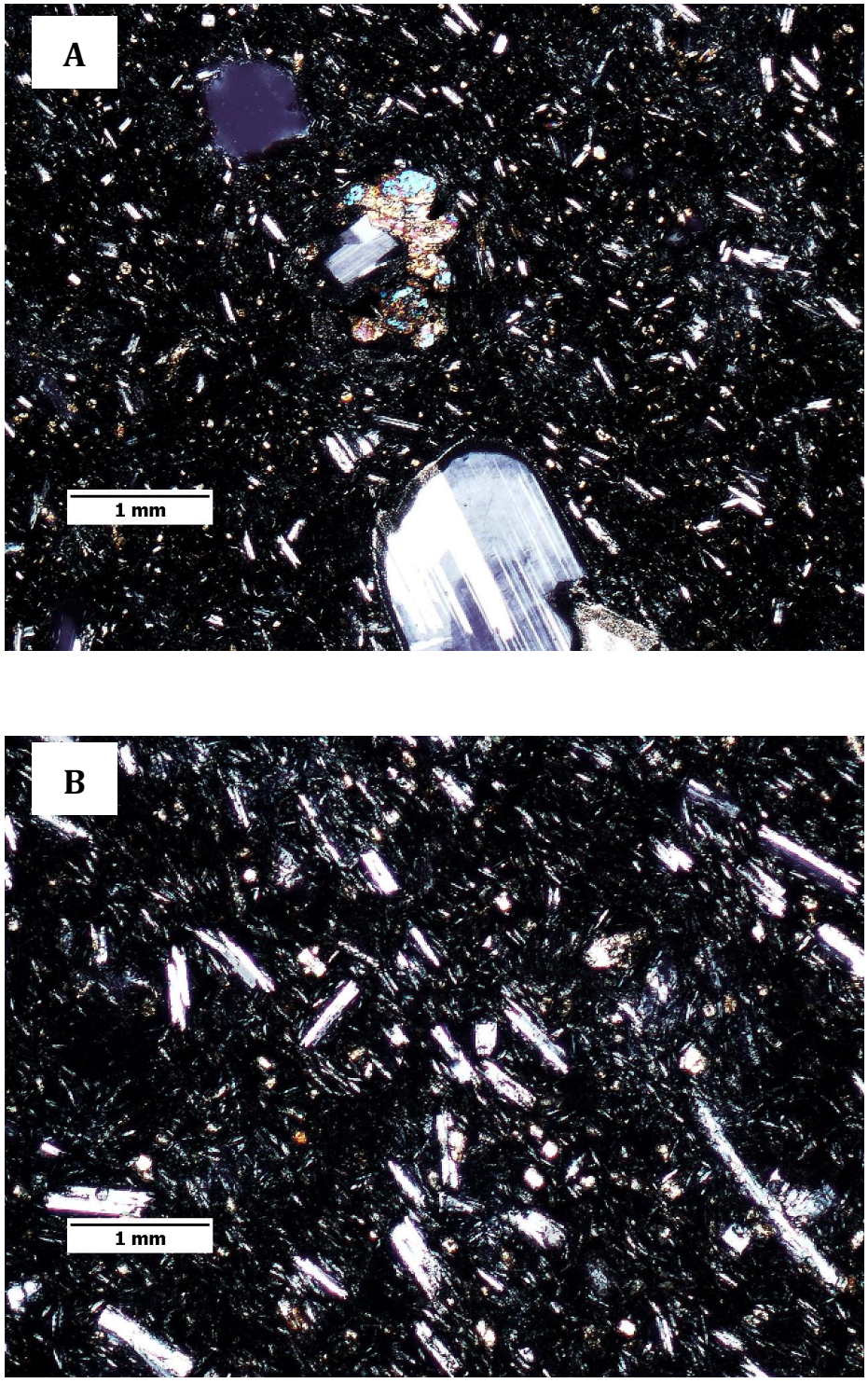

Fig. 3. Photomicrographs of Dayingshan basaltic andesite. A) 4X view showing large phenocrysts of olivine (middle center) and plagioclase (bottom center). B) 10X view of the groundmass showing dominantly plagioclase laths in a dark matrix.

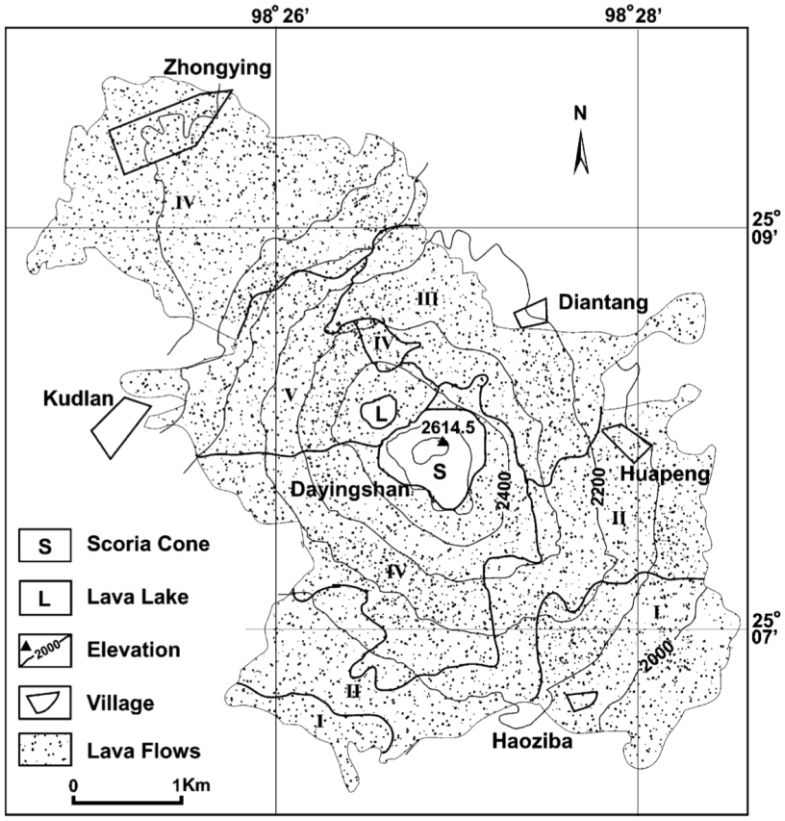

Fig. 4. Distribution of depositional units deposited by multiple eruptive events from Dayingshan volcano. I is the oldest flow, and V is the youngest. A small lava lake has developed to the northwest of the scoria cone (From Wei et al., 2002).

Concerning Zircon

Zircon ($ZrSiO_4$) is a common accessory mineral that forms in rocks all over the world. Zircon crystals can be found in sedimentary, metamorphic, and igneous rocks, and are mostly known for their importance to geochronology and crustal evolution studies. The most important reason zircons are useful in geochronology is because they typically contain radioactive uranium, often leading to metamictization of the mineral, and they incorporate very little lead. Radioactive elements such as uranium retain information that is critical for understanding the nature, origin, and age of a particular rock. Zircon has a strong, tetragonal, prismatic crystal structure and a hardness of 7.5 (Perkins, 2002), which contributes to the extreme durability of the mineral. In fact, zircons are so resilient to weathering that they have been found in terrestrial Earth samples to be as old as 4.404 ± 9 Ga (Wilde, 2001). Zircons are also stable in temperatures up to 1690°C and pressures up to 4.8 GPa (Finch & Hanchar, 2003). This stability in extreme temperatures and pressures allows zircon minerals to endure most metamorphic processes without changing the composition.

This research focuses on the occurrence of zircon in fresh igneous rocks. Unlike dating zircon from detrital or metamorphic rock, the dating of zircon in an igneous rock yields the age at which the rock cooled from a melt. The volcanic rocks produced at Dayingshan are fairly silica-rich, which is an important factor in zircon production. Zircons are most common in igneous rocks of intermediate to Si-saturated composition and least common in less Si-saturated rocks, such as basalts (Hoskin & Schaltegger, 2003). Zircons in extrusive volcanic rocks tend to crystallize rapidly, resulting in relatively small crystals that typically show an acicular habit, with length to width ratios

up to 1:12 (Hoskin & Schaltegger, 2003). A common texture seen in igneous zircons is growth zoning. Zoning records different crystallization events throughout the life of the zircon, recording and preserving thermal events from tens to millions of years. With the development of mass spectrometry, geologists can obtain the approximate ages of these different crystallization events.

The current study attempts to use zircon to investigate igneous processes such as magma chamber storage time and the use of zircon as a possible provenance-indicator. Zircons must be extracted from the source rock and dated in order to attain their early pre-eruptive crystallization age, which corresponds with early magma chamber evolution. In intermediate to felsic magmas, zircons will typically crystallize and remain suspended in a melt for time periods greater than 100 ka (Simon et al., 2008). When a melt rises from great depth and reaches the magma chamber, it begins to cool. At temperatures of ~800°C, zircons dissolve fairly rapidly into a hydrous melt (Reid et al., 1997). Therefore, the ages obtained from the zircons reflect the last time the melt cooled through this temperature. Consequently, it can be concluded that zircon crystallization ages date the cooling of magma to its zircon saturation temperature, which can be determined based on U-Th disequilibrium measurements (Reid et al., 1997). Magma storage time can thus be discerned by subtracting the age of the last eruption event from the age of the zircons in the sample rock; however, it must first be determined that the zircons grew in the magma body during the build-up to eruption. Because the ability to resolve age differences decreases with rock age, the most informative data about residence time scales come from young eruptions (Simon et al., 2008).

Using zircons to determine magma provenance is more complicated. In order to do so, one must relate the atomic composition of zircon to lithology. Several studies have had moderate success, such as Heaman et al. (1990), who used plots of Lu, Sc, Th/U and Lu/Sm versus Hf to relate zircons to several specific environments, and Hoskin & Ireland (2000), who studied the rare earth element (REE) abundance differences in zircons from mantle-derived rock and compared those with crustal zircons. The relationship between certain REE abundances and their derivation from a crustal or mantle source provides strong evidence for the origins of the melt. Ultimately, there is no clear, defining relationship between igneous zircon composition and magmatic source. For whole-rock U-series data, pronounced ^{230}Th excesses in young (< 350 ka) volcanic rocks may indicate the lavas were produced from a deep mantle source (Zou & Fan, 2010). On the other hand, ^{238}U excesses are attributed to the addition of fluids from the subducting plate into the mantle wedge (i.e. subduction zones) or shallow mantle melting of a spinel peridotite source.

Uranium-Series Radiometric Dating

Radiometric dating works on the principle that radioactive parent isotopes decay at constant rates through time into daughter isotopes. While the decay of one particular isotope is spontaneous, probability dictates that a large population of isotopes decay at regular rates known as half-lives. The half-life of a decay pair is the time it takes for half of the parent isotopes to decay into stable daughter isotopes. The rate of decay depends only on the properties of the isotope, and is not affected by environmental factors such as temperature and pressure. This constant rate of decay allows for the parent-daughter ratio

to be used as a clock to measure the time that has elapsed since the crystal formed. An assumption must be made that the crystal has a closed system to temperature and pressure. Because alteration can sometimes be detected through geologic evidence or growth zoning, and using more than one parent-daughter system can commonly be used to cross-check ages, this assumption can often be made confidently. The resilience of zircon to alteration due to environmental changes also provides confidence in this assumption. Some minerals may incorporate daughter isotopes into the original composition. In this case, an isochron method must be applied to attain crystal age.

Uranium-series dating is the most commonly used isotopic series in radiometric dating for several reasons. The first is that it has several intermediate isotopes with a range of half-lives before it reaches its final decay product of Pb, providing several useful time frames for dating. For example, ^{238}U-^{230}Th has a half-life of 75,690 years, while ^{238}U-^{206}Pb has a half-life of 4.5 billion years. Because most accessory minerals incorporate little to no lead, ages based on the latter decay pair are widely accepted. Figure 5 follows the ^{238}U parent isotope and its decay into several intermediate daughter isotopes.

Radiometric dating assumes a closed system. Although a closed system assumption is sometimes contested, it is widely accepted for zircon U-series dating because elements are immobile in zircon even at magmatic temperatures (Schmitt, 2009). This closed system can be disturbed by partial melting, and the reader is referred to the book, *Quantitative Geochemistry*, by Zou (2009) for models that relate the extents of U-series decay to the melting process as it pertains to elemental partition coefficients, melting porosity, melting rate, and melting time.

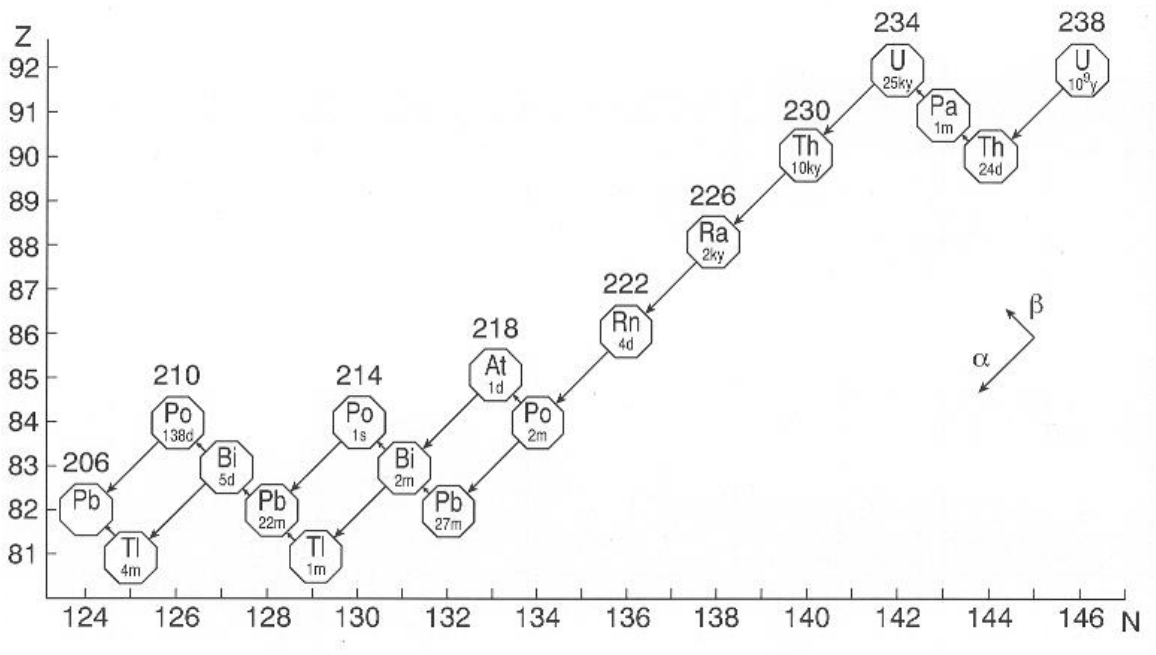

Fig. 5. ^{238}U decay chain depicting either alpha or beta decay into several intermediate isotopes before the final stable ^{206}Pb isotope is reached. N = atomic number; Z = atomic mass (From Berg, 2008).

While several uranium decay series may be used to radiometrically date zircons, the most proficient and well-known are the two U-Pb series due to long half-lives. Another reason for the wide use of zircon U-series dating is that it has two clocks. Essentially, the decay of both the ^{238}U and ^{235}U isotope allow for the ability to cross-check and confirm age data. Other commonly used U-series decay pairs in geology are U-Th, Th-Ra and U-Pa. Because Dayingshan volcanic rocks are geologically young, the ^{238}U-^{230}Th decay pair is most appropriate. The half-life of the ^{238}U-^{230}Th decay pair is 75,690 yrs, which results in a maximum attainable age of ~350 ka (Schmitt, 2009). Mass spectrometry can be used to measure the approximate parent to daughter ratios of ^{238}U-^{230}Th. Because ^{230}Th abundances are especially low in upper Quaternary rocks, an instrument with low background noise and high sensitivity is ideal.

Secondary Ion Mass Spectrometry (SIMS)

SIMS is a radiometric dating technique that measures the composition of solid materials on a micron scale, and is most commonly performed with an ion microprobe. SIMS main strengths are in trace element quantification due to low backgrounds and high sensitivity (Stern, 2009). The target zircon is initially sputtered with a high-energy beam of primary oxygen ions ($^{16}O_2^-$ or $^{16}O^-$) that causes some of the atoms and molecules of the zircon to become ionized (Fig. 6). The secondary ions, which have been sputtered off the target zircon and thus represent the zircon composition, are separated by a mass spectrometer and counted by secondary ion detectors (Ireland and Williams, 2003).

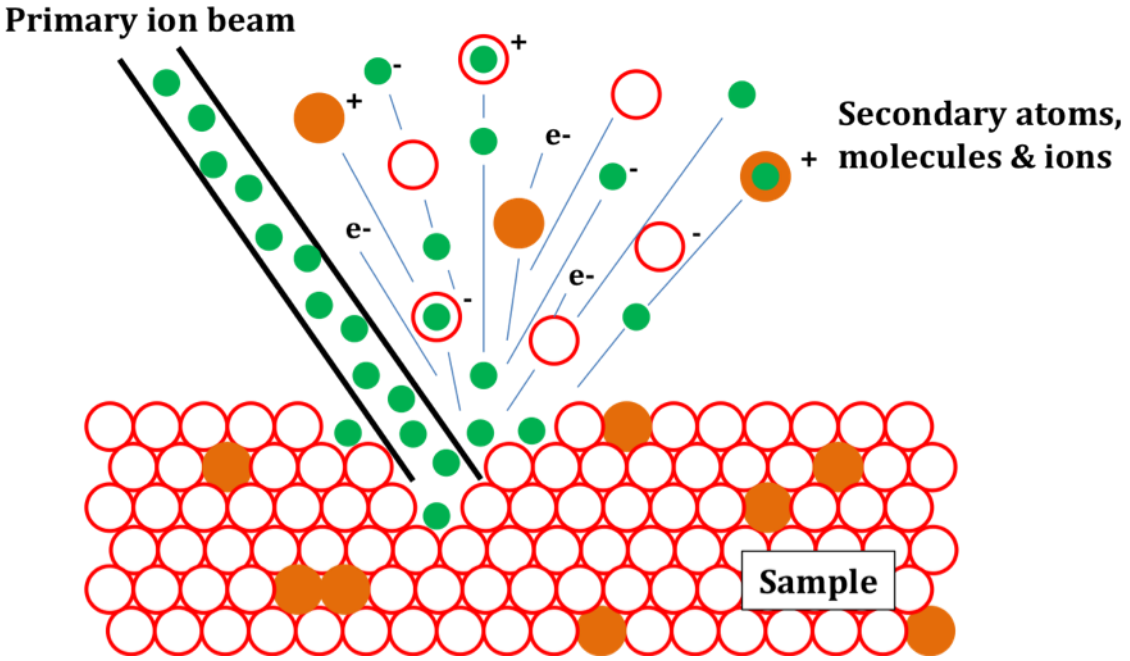

Fig. 6. Diagram depicting a sample being sputtered by a beam of primary ions, resulting in the backscatter of secondary atoms, molecules, and ions (After Evans Analytical Group LLC, 2010).

Erroneous data may be recorded from SIMS due to any number of different instrumental and sample preparation errors, which will be discussed in greater detail below. To make certain these errors are not occurring, multiple zircon standards (e.g., AS-3 from the Duluth anorthosites) are mounted along with the unknown zircon samples. Standards are zircons from rocks of a known age. By using SIMS on these standards, one can determine if there is an error in the machine and make the necessary adjustments to correct the error. Zircon standards are especially necessary to correct for mass discrimination of U, Th, and Pb.

SIMS is the least destructive of the radiometric dating techniques, creating a crater 10-50 μm in diameter with an approximate depth of < 5 μm (Ireland & Williams, 2003). Amount of sample destruction is much less than comparable dating techniques such as Laser Ablation Inductively Coupled Plasma Mass Spectrometry (LA-ICPMS) and Thermal Ionization Mass Spectrometry (TIMS) (Fig. 7). There is also very little heating and vaporization due to a much lower amount of energy absorbed by the target (Stern, 2009). SIMS high spatial resolution allows for the targeting of specific growth zones on the zircon crystal.

The use of SIMS in Quaternary-age materials is a relatively new approach in the field of geochronology. High sensitivity and micrometer-scale spatial resolution make SIMS a premier tool in Quaternary geochronology, as the useful yield of U-series isotopes is typically low in rocks so young. SIMS, coupled with imaging techniques such as backscattered electron (BSE) imaging and cathodoluminescence (CL), allows the user to finely target specific regions on a crystal surface for chemical and isotopic analysis (Ireland & Williams, 2003). Depth profiling, another SIMS technique, enhances the

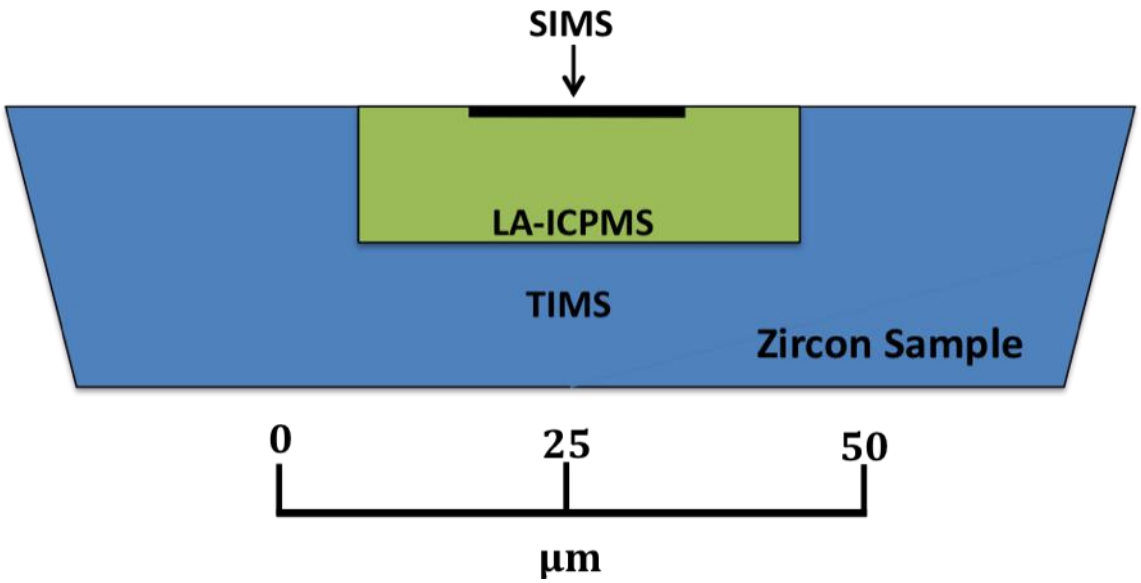

Fig. 7. Diagram depicting average zircon sample destruction area of SIMS, LA-ICPMS, and TIMS in cross-section view. SIMS spot size is typically 10-20 µm and <2 µm depth. LA-ICPMS spot size is typically 30-60 µm and 10-20 µm depth. TIMS analysis consumes the sample in its entirety (After Košler & Sylvester, 2003).

spatial resolution to several micrometers, which also aids in obtaining crystallization ages in zoned zircons.

An isochron method must be applied in order to ultimately attain rock age due to the fact that zircon may initially incorporate ^{230}Th into the system. An isochron is a straight line plotted on a D_r/D_n versus P/D_n diagram. This method works on the assumption that the ratio of a radiogenic daughter isotope (D_r), formed by the decay of a parent isotope (P), to a related nonradiogenic isotope (D_n) was initially the same for each zircon analyzed. The age is ultimately attained by measuring the slope of the isochron, which increases with age. The isochron method is useful because it determines the initial amount of radiogenic daughter isotopes; therefore, no assumptions of the initial amount of daughter isotopes need be made. For zircons from Dayingshan, an isochron is plotted on a (^{230}Th)/(^{232}Th) vs. (^{238}U)/(^{232}Th) diagram. One can develop an isochron in two ways: (1) by using the two-point model isochron method using zircon melt-pairs, or (2) by using internal isochrons for multiple spots on single or multiple crystals (Schmitt, 2009). The following equation is used to construct an isochron (λ = decay constant; t = time between radioactive disequilibrium generation event and current measurement):

$$\frac{\left(^{230}Th\right)}{\left(^{232}Th\right)} = \frac{\left(^{238}U\right)}{\left(^{232}Th\right)}\left(1 - e^{-\lambda_{230}t}\right) + \frac{\left(^{230}Th\right)^{0}}{\left(^{232}Th\right)}e^{-\lambda_{230}t}$$

The age can then be calculated from the slope (m) of that line using the following equation:

$$t = \frac{\ln\left(1 - m\right)}{\lambda_{230}}$$

Figure 8 is an isochron diagram of zircons collected from Puy de Dome, a large lava dome in south-central France, illustrating both the two-point model isochron method and an internal isochron for multiple spots on single crystals (Schmitt, 2009). The two-point model isochron method using zircon-melt pairs is used if uranium-series isotope abundances are too low. For Dayingshan zircons, the internal isochron method is applied; however, because of the small size of the zircons, isochrons are determined based on single spots on multiple crystals.

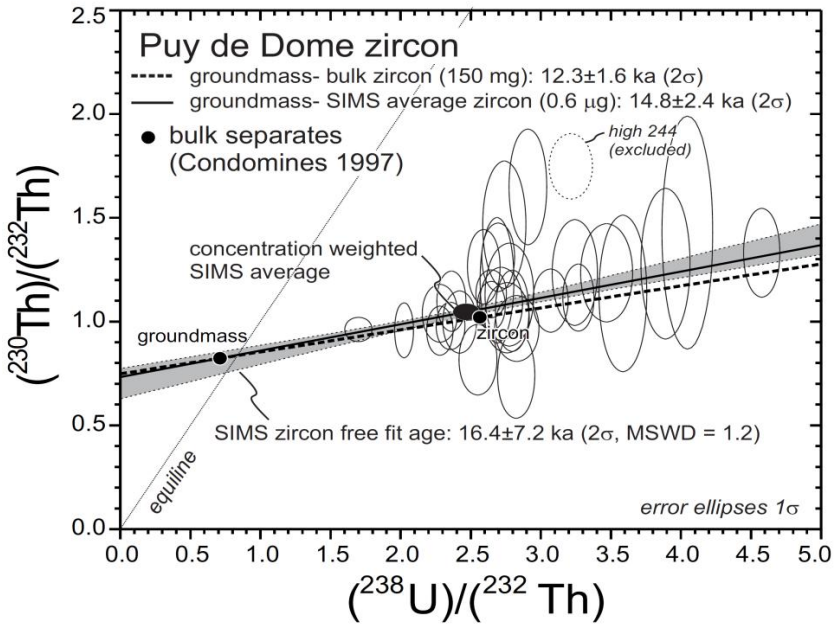

Fig. 8. Isochron diagram illustrating both the two-point model isochron method (dashed line) and internal isochron for multiple spots on single crystals (solid line) (From Schmitt, 2009). A comparison with bulk TIMS data (Condomines, 1997) is also provided.

PREVIOUS WORK

Some of the first isotopic and geochemical work done in the Tengchong volcanic field was performed by Zhu et al. (1983). They recognized that the compositions of the volcanic rocks in the area were complex and changed over time. The wide range of volcanic compositions were observed and separated into five groups belonging to three series: a major series (high-Al basalts), an andesite-dacite series, and a high-Mg series. Isotopic analysis indicated an enriched mantle source attributed to older subducted components (subduction prior to Indian-Eurasian plate collision). The same authors also noted that the most recent volcanics seemed closely linked to the tectonic environment. Periods of extensional regimes are marked by more frequent eruptions, while periods of compressional regimes are marked by pauses in volcanic activity.

Wang, Y. et al. (2006) expanded on tectonics as the controlling factor for volcanic activity. Based on the timing of faulting and basin formation, analysis of the cooling history of the mountain belt, and calculations of seismic foci, they concluded that the magma formed as a result of collisional orogenic processes, but strike-slip motion of the Saigang fault is the biggest factor that controls volcanic eruptions.

Wang, F. et al. (2006) noted enriched mantle characteristics in the Tengchong volcanic rocks, and concluded that the enrichment was due to partial melting of a metasomatized mantle source. Wang, F. et al. (2006) were also the first to measure U and Th isotopes in the Tengchong volcanic field, and determined from these measurements that there was probably some heterogeneity in the source. They concluded

that there are two possible source domains for the lava; (1) an LREE-enriched, high Rb/Sr end-member, and (2) a second end-member representing a more typical arc-type melt. Another important focus in this study was the authors attempt to put constraints on magma chamber storage time. This was done based on U-Th and $^{40}Ar/^{39}Ar$ age dating, but results were inconclusive as different ages (~77 ka for U-Th; ~32.2 ka for $^{40}Ar/^{39}Ar$) were calculated from the same crystal using these two techniques. Wang, F. et al. (2006) only worked on major minerals, and these rock-forming minerals have relatively low U and Th concentrations. Their data is therefore subject to high errors and inconsistencies.

Zou et al. (2010) focused more on the times scales and nature of magma storage, using U-Th dating of zircons from Maanshan volcano to calculate magma storage time. Unlike Wang, F. et al. (2006), Zou et al. (2010) were able to separate measured zircons into two populations by utilizing SIMS. A magma storage time of 45 ka was determined for the most recent eruption. Due to bi-modal zircon ages, it was concluded that the older age population (~91 ka) represented remobilized zircon antecrysts from an earlier phase of magmatism, while the younger population (~55 ka) grew in the magma body itself prior to eruption. The study also concluded based on zircon saturation calculations that there are no inherited zircons from country rocks in the most recent lava flows.

METHODS

Zircon Extraction

The initial stage in this research was to extract zircon crystals from a volcanic rock sample from Dayingshan (sample # TC09026). The first step in the zircon extraction process is to crush and grind the rock into particles approximately 25-50 μm in diameter. This was the approximate particle size at which the rock became disaggregated. Crushing was done using a rock hammer and laboratory disc mill. The rock hammer was used to break the rock into pieces small enough to feed into the disc mill, which then ground the rock into smaller (~25-50 μm) particles. While breaking the rock with a rock hammer, a box was used to contain the broken rock fragments. The ceramic laboratory disc mill used to grind the sample further was brand new, and thus contained no contaminants. After grinding to the appropriate size, the sample was then decanted with water to separate some of the lighter minerals from the heavier minerals. Minerals that remained in suspension in the water were poured off (e.g., mica), while the denser minerals, such as zircon, sank in the water. A high-powered hand magnet was then repeatedly used to draw off metallic minerals.

The next step is heavy liquid separation, which is used to separate out only the heaviest minerals (e.g. zircon). The heavy liquid separation process was done using the facilities and equipment of Columbus State University. The heavy liquid used was methylene iodide (MEI). MEI (CH_2I_2) is a good liquid to use because it has a relatively high specific gravity of 3.335. Because zircon has a specific gravity of 4.68 (Perkins,

2002), zircon sinks in the MEI while lighter minerals float to the top. After mixing a small amount of the rock sample into the MEI in a separatory funnel, a 24-hour time period was allowed to elapse, giving the heavy minerals sufficient time to sink through the heavy liquid. After 24 hours, the MEI at the bottom of the separatory funnel, which held the heaviest minerals, was poured out onto filter paper. The sample was then washed in acetone and dried in an oven in order to drive off the last remaining MEI.

The last step in the zircon extraction process was to pick out the zircons from the other heavy minerals separated out by the heavy liquid. This was carefully and meticulously done using a fine-point needle under an optical microscope. The entire process was repeated several times over the course of two weeks until a sufficient number of zircons were recovered (~30).

Sample Preparation

After the separation process, the zircons must be prepared and mounted specifically for SIMS. Proper sample preparation is of the utmost importance for SIMS. Secondary ion yields are sensitive to local topographic and electrostatic features of the sample mount (Stern, 2009). The crystals are first embedded in indium, washed in dilute HCl, and plated with a thin (20-40 nm) gold layer to generate a conducting sample surface (Fig. 9). Indium is a soft metal that is used instead of traditional epoxy to minimize potential interferences on ^{230}Th isotopes from the matrix. The unpolished mount is then placed in a sample holder, the standard dimensions of which are ~ 1 inch in diameter with a thickness of ~1/2 cm (Schmitt, 2009). A nonmagnetic spring and backing plate hold the sample in place (Fig. 10). The sample is unpolished because unpolished zircons allow for

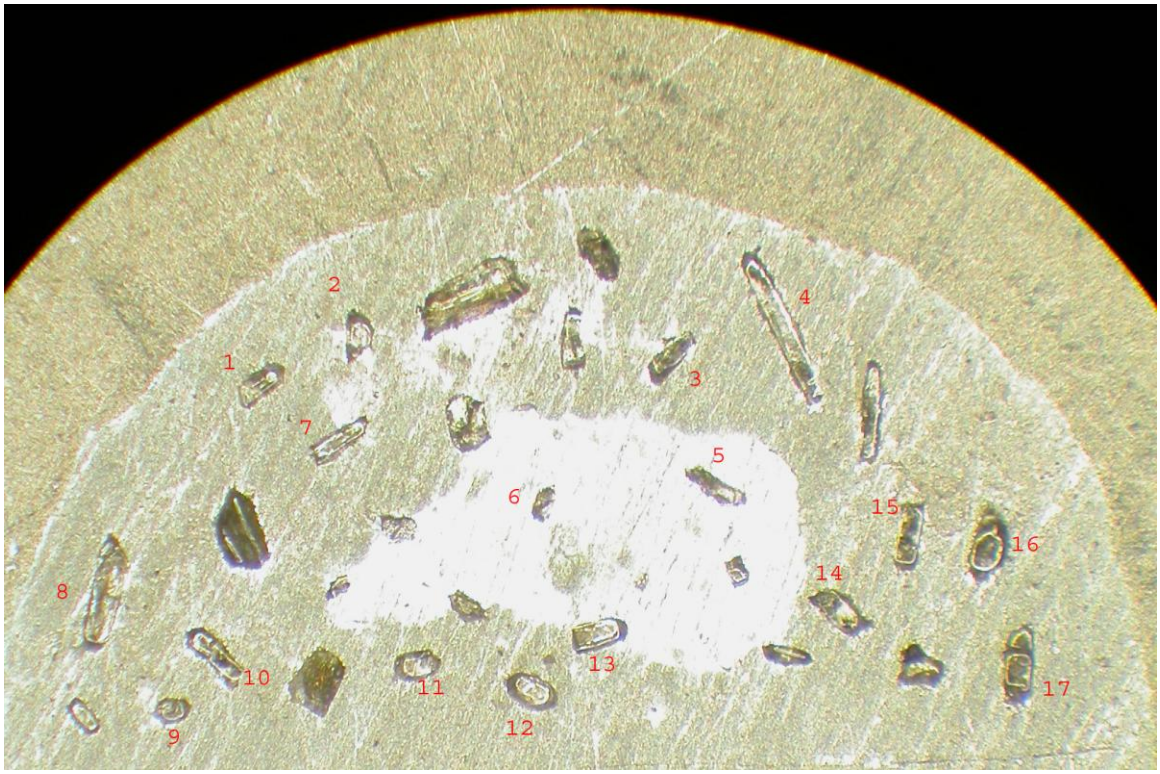

Fig. 9. Final mount of Dayingshan zircons after having been pressed into indium and coated in a thin layer of gold. Zircons were later numbered by a computer in the order in which they were sputtered.

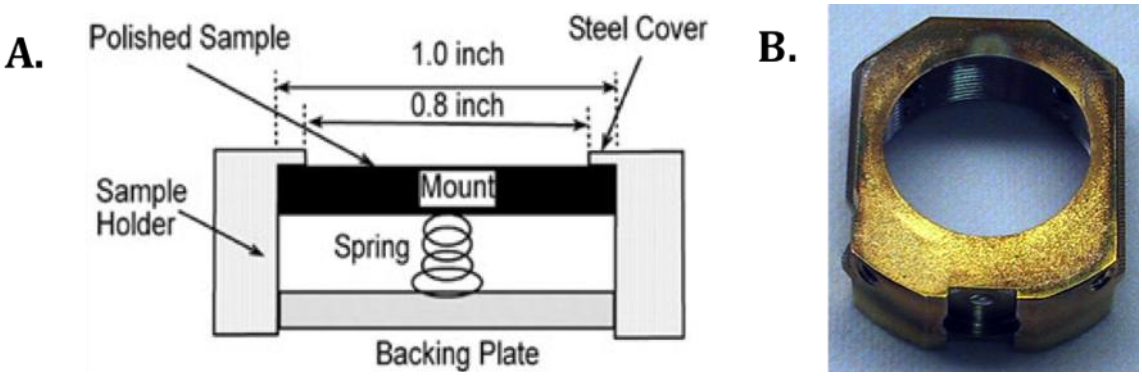

Fig. 10. A.) Schematic diagram of a sample holder showing the backing plate and spring. Note that the amount of mount surface area available for analysis is decreased by 0.2 inches after insertion into the sample holder. B.) Photograph of a standard sample holder (From UCLA, 2010).

shallow depth profiling which provides enhanced spatial resolution on natural crystal surfaces. After the mount is inserted into the sample holder, the sample holder must be inserted into the instrument through an airlock system as the ion probe is kept under Ultra High Vacuum (UHV). The sample was then sputtered with a primary beam of $^{16}O^-$ ions generated in the duoplasmatron in order to obtain rim ages. The duoplasmatron works by converting gas into an ion beam. Zircon sputter rates are ~0.05 μm^3/nA/sec (Schmitt, 2003), and the typical time required to sputter one zircon is ~20 minutes.

After sputtering the unpolished zircons, the sample was then removed from the machine, polished using a diamond polishing compound, cleaned with dilute HCl, and coated with another thin Au layer. Zircons were then sputtered again to obtain core ages. Because a relatively flat crystal face is needed in order to accommodate the ion beam, it is important to note that fewer zircons were measured during the unpolished measurements due to a smaller percentage of zircon surface area. The zircons initially pressed into the Indium may or may not yield a flat crystal surface for measuring. Upon completion, the final zircon mount, containing the polished zircons with SIMS craters, was kept for potential future analysis.

Cameca ims 1270 Analytical Methods

Measurements for this research were done using the Cameca ims 1270 at the NSF National Ion Microprobe Facility at the University of California, Los Angeles (UCLA) (Fig. 11). The facility was commissioned as a national facility in 1996, and scientists have generated over 300 publications using UCLA SIMS data (UCLA, 2011). $^{230}Th/^{232}Th$ and $^{238}U/^{232}Th$ analyses with the Cameca ims 1270 achieves an average precision of

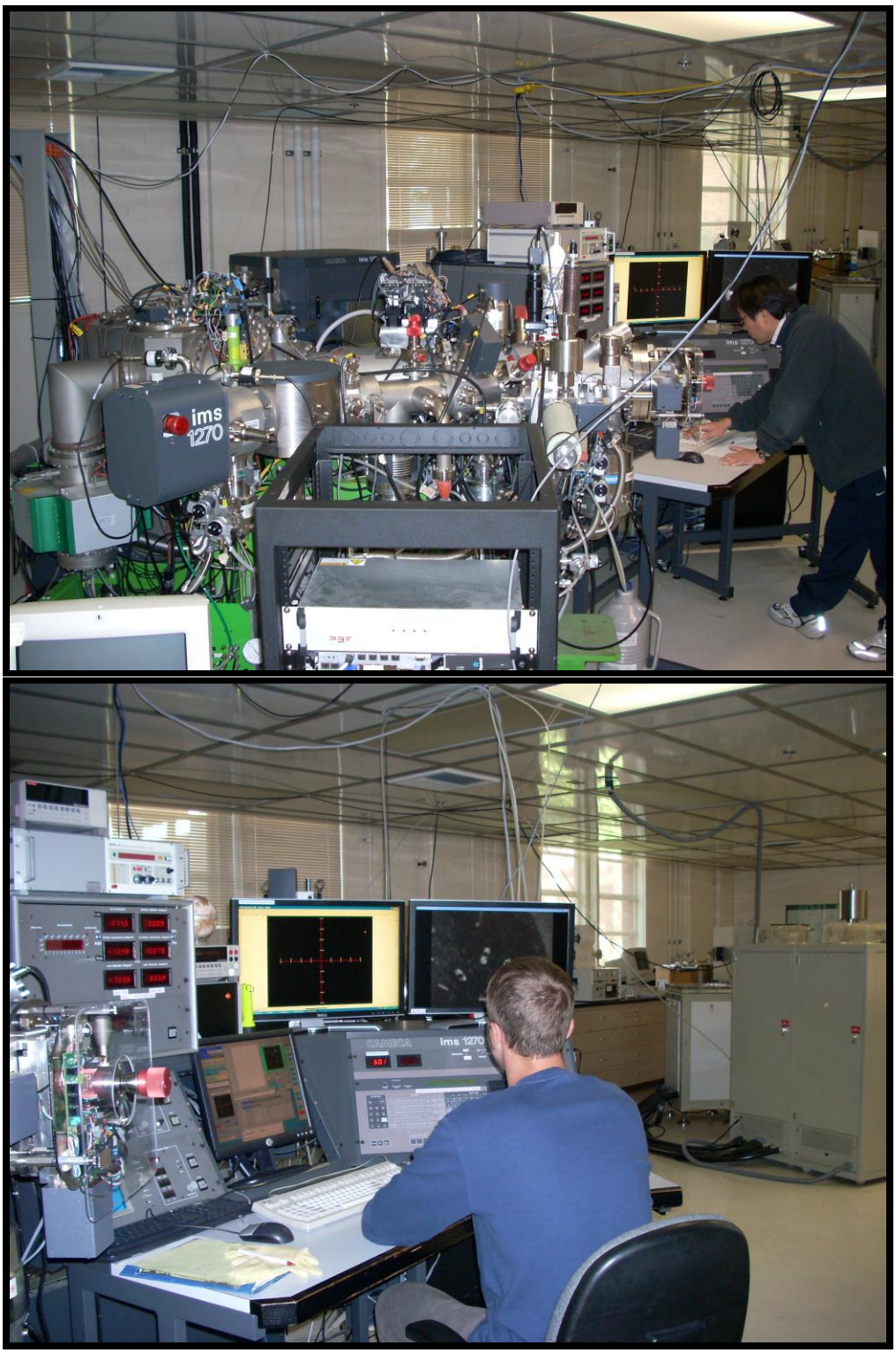

Fig. 11. Top - Photograph of the Cameca ims 1270 at the NSF National Ion Microprobe Facility at UCLA. Bottom - Author at control console of the Cameca ims 1270.

~1-2 % (Zou et al., 2010). $^{230}Th/^{232}Th$ and $^{238}U/^{232}Th$ analyses with the Cameca ims 1270 achieves an average precision of ~1-2 % (Zou et al., 2010). There are several SIMS instruments and analytical approaches; however this paper will only address the operational procedures for the Cameca ims 1270. Techniques for other SIMS instruments may vary, and the reader is referred to Ireland & Williams (2003) for operation and techniques of some of these other instruments (i.e. SHRIMP I and SHRIMP II). Figure 12 represents a 3D schematic of the Cameca ims 1270.

The most important secondary ion intensities measured by SIMS U-Th dating are $^{230}Th^{16}O+$, $^{232}Th^{16}O^{+}$, and $^{238}U^{16}O^{+}$. Oxides are measured because they typically show higher intensities than metals. Ultimately, the counts of these three oxides are used to calculate the age of the crystal. $^{90}Zr_2{}^{16}O_4{}^{+}$ is also measured as a reference. These ions are measured both individually and against background measurements, and are gain corrected to ensure accurate counts and calibration. The raw data for measured Dayingshan zircons are presented in Table 2. AS-3 zircons from the Duluth Complex were used as standards to calibrate the relative sensitivities for ^{238}UO, ^{232}ThO and ^{230}ThO. Radiogenic $^{206}Pb/^{208}Pb$ is measured in the AS-3 zircons rather than Th/U because in old, concordant zircons with known ages, the radiogenic $^{208}Pb/^{206}Pb$ is a unique function of the Th/U atomic ratio (Zou et al., 2010); therefore, a Th/U relative sensitivity factor can be calculated. The primary current was generated at ~40-80 nA, and the secondary ions were analyzed at a mass resolving power of ~5000.

SIMS works by sputtering the target sample with a primary beam of either $^{16}O_2{}^{-}$ or $^{16}O^{-}$ ions. This beam is generated using a duoplasmatron, which converts the gas into

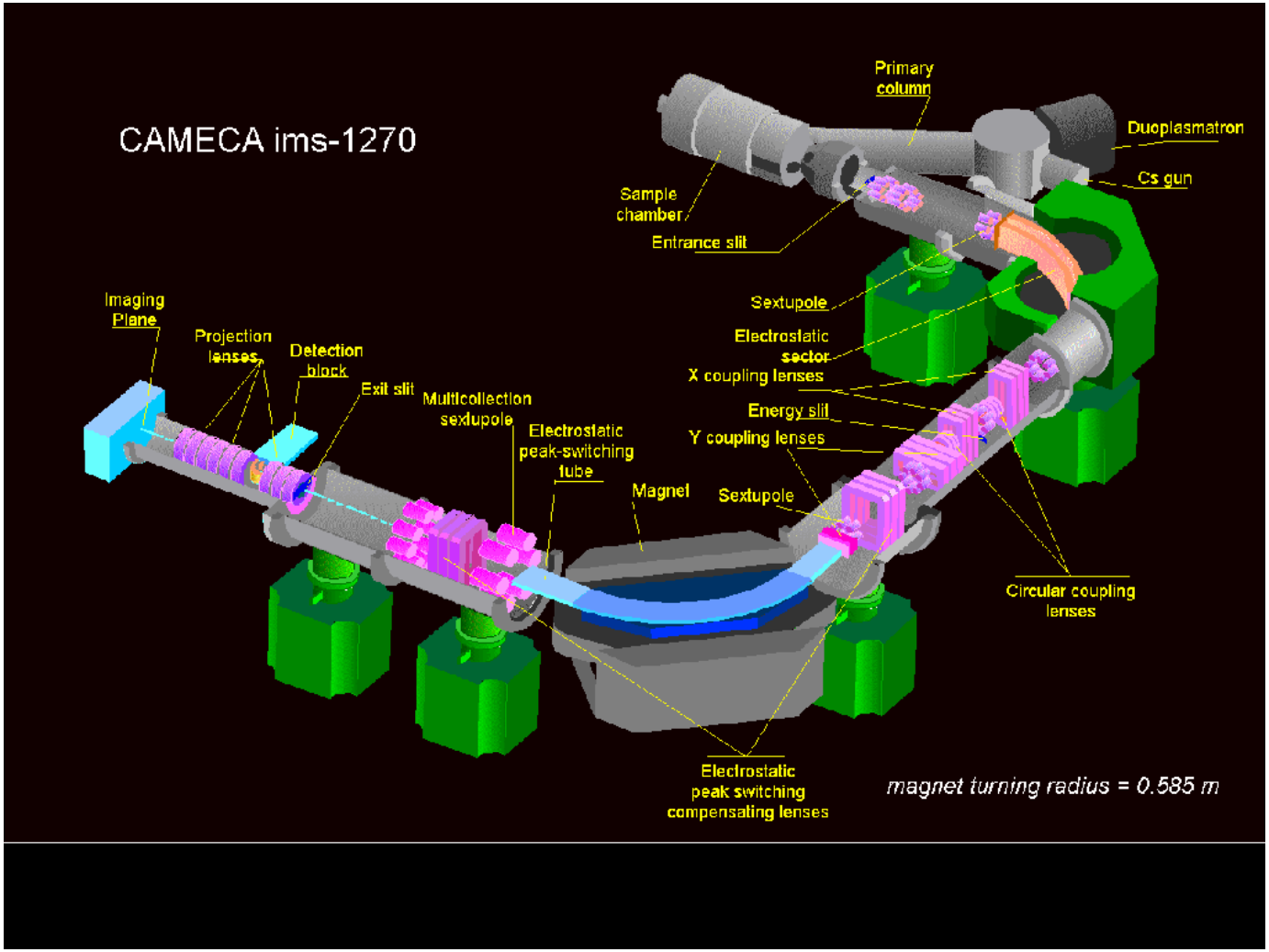

Fig. 12. 3D schematic of CAMECA ims-1270 instrument and its components (From UCLA, 2011).

Table 2
Raw data for Dayingshan zircon rims and cores collected from SIMS analyses. 1 s.e. is the standard error, which represents measurement uncertainty. Background is measured at 246.3 and 244.038, respectively.

Sample	*246.02804/*	*246.02804/*	*U O/*	*U O/*	*246.02804/*	*246.02804/*
	U O	*U O*	*Th O*	*Th O*	*Th O*	*Th O*
		1 s.e.		**1 s.e.**		**1 s.e.**
Day_rim_z@1	1.29E-05	7.31E-07	1.56E+00	5.54E-03	2.01E-05	1.07E-06
Day_rim_z@2	1.08E-05	3.12E-07	5.52E-01	1.03E-02	5.95E-06	1.81E-07
Day_rim_z@3	1.06E-05	4.19E-07	6.55E-01	6.15E-03	6.96E-06	2.74E-07
Day_rim_z@4	1.21E-05	5.87E-07	8.45E-01	5.47E-03	1.02E-05	4.84E-07
Day_rim_z@5	7.98E-06	2.55E-07	1.11E+00	1.86E-02	8.84E-06	2.82E-07
Day_rim_z@6	1.03E-05	2.99E-07	5.92E-01	2.38E-03	6.12E-06	1.77E-07
Day_rim_z@7	1.44E-05	7.72E-07	3.08E-01	4.30E-03	4.45E-06	2.66E-07
Day_rim_z@8	1.04E-05	3.51E-07	6.23E-01	1.93E-02	6.45E-06	2.50E-07
Day_rim_z@9	1.16E-05	3.50E-07	4.94E-01	3.06E-03	5.72E-06	1.73E-07
Day_rim_z@10	9.24E-06	3.49E-07	8.33E-01	1.35E-02	7.71E-06	3.28E-07
Day_rim_z@11	1.02E-05	3.61E-07	9.76E-01	9.08E-03	9.95E-06	3.53E-07
Day_rim_z@12	1.02E-05	2.61E-07	7.69E-01	3.36E-03	7.81E-06	1.91E-07
Day_rim_z@13	8.62E-06	2.46E-07	9.12E-01	6.78E-03	7.84E-06	2.10E-07
Day_rim_z@14	1.06E-05	3.68E-07	7.21E-01	3.75E-03	7.65E-06	2.66E-07
Day_rim_z@15	1.08E-05	4.50E-07	6.30E-01	1.17E-02	6.78E-06	3.05E-07
Day_rim_z@16	1.11E-05	5.20E-07	9.37E-01	7.12E-03	1.04E-05	4.86E-07
Day_rim_z@17	1.08E-05	3.36E-07	5.03E-01	3.41E-03	5.45E-06	1.73E-07

Table 2 continued
Raw data for Dayingshan zircon rims and cores collected from SIMS analyses. 1 s.e. is the standard error, which represents measurement uncertainty. Background is measured at 246.3 and 244.038, respectively.

Sample	*246.3/*	*246.3/*	*246.3/*	*246.3/*	*244.0381/*	*244.0381/*
	U O	*U O*	*Th O*	*Th O*	*U O*	*U O*
		1 s.e.		**1 s.e.**		**1 s.e.**
Day_rim_z@1	2.39E-07	7.85E-08	3.75E-07	1.23E-07	2.43E-06	3.20E-07
Day_rim_z@2	4.64E-07	1.59E-07	2.55E-07	8.52E-08	7.06E-07	8.07E-08
Day_rim_z@3	5.29E-07	3.36E-07	3.33E-07	2.07E-07	6.38E-07	1.08E-07
Day_rim_z@4	1.06E-06	5.38E-07	9.17E-07	4.69E-07	2.59E-06	3.75E-07
Day_rim_z@5	1.34E-07	6.77E-08	1.51E-07	7.66E-08	3.55E-07	5.38E-08
Day_rim_z@6	3.35E-07	1.35E-07	1.97E-07	8.02E-08	7.99E-07	8.18E-08
Day_rim_z@7	1.17E-06	4.05E-07	3.50E-07	1.21E-07	1.27E-06	1.84E-07
Day_rim_z@8	6.03E-07	3.87E-07	3.37E-07	2.05E-07	6.03E-07	8.58E-08
Day_rim_z@9	2.20E-07	9.71E-08	1.08E-07	4.79E-08	8.14E-07	1.05E-07
Day_rim_z@10	3.79E-07	1.48E-07	3.05E-07	1.20E-07	5.23E-07	9.12E-08
Day_rim_z@11	3.50E-07	1.46E-07	3.37E-07	1.40E-07	9.60E-07	1.11E-07
Day_rim_z@12	2.75E-07	8.59E-08	2.13E-07	6.67E-08	8.22E-07	9.80E-08
Day_rim_z@13	3.91E-07	1.65E-07	3.51E-07	1.47E-07	4.02E-07	4.97E-08
Day_rim_z@14	7.52E-07	3.97E-07	5.34E-07	2.83E-07	3.48E-07	6.71E-08
Day_rim_z@15	4.64E-07	2.63E-07	3.08E-07	1.84E-07	6.93E-07	1.07E-07
Day_rim_z@16	2.04E-07	1.81E-07	1.95E-07	1.71E-07	7.97E-07	1.39E-07
Day_rim_z@17	2.66E-07	1.02E-07	1.33E-07	5.08E-08	5.45E-07	6.98E-08

Table 2 continued
Raw data for Dayingshan zircon rims and cores collected from SIMS analyses. 1 s.e. is the standard error, which represents measurement uncertainty. Background is measured at 246.3 and 244.038, respectively.

Sample	*244.0381/*	*244.0381/*	*U O/*	*U O/*	*246.3*	*92Zr Zr O4*
	Th O	*Th O*	*Zr2 O4*	*Zr2 O4*		
		1 s.e.		**1 s.e.**		
Day_rim_z@1	3.75E-06	4.83E-07	1.42E+01	7.16E-01	0.1706	2.98E+04
Day_rim_z@2	3.96E-07	4.75E-08	1.32E+01	3.60E-01	0.184	1.79E+04
Day_rim_z@3	4.13E-07	6.88E-08	5.32E+00	9.09E-02	0.1227	2.48E+04
Day_rim_z@4	2.18E-06	3.14E-07	5.95E+00	6.08E-02	0.161	1.95E+04
Day_rim_z@5	4.00E-07	6.06E-08	1.05E+01	1.33E-01	0.05745	2.55E+04
Day_rim_z@6	4.71E-07	4.82E-08	8.92E+00	2.76E-01	0.1284	3.37E+04
Day_rim_z@7	3.90E-07	5.64E-08	3.82E+00	3.78E-02	0.1494	2.21E+04
Day_rim_z@8	3.61E-07	5.14E-08	6.46E+00	2.70E-01	0.1513	2.74E+04
Day_rim_z@9	3.99E-07	5.04E-08	9.46E+00	2.16E-01	0.06894	2.32E+04
Day_rim_z@10	4.47E-07	8.26E-08	7.81E+00	7.00E-02	0.1015	2.10E+04
Day_rim_z@11	9.45E-07	1.09E-07	7.76E+00	3.56E-02	0.09388	2.29E+04
Day_rim_z@12	6.25E-07	7.12E-08	1.41E+01	4.89E-01	0.1725	2.70E+04
Day_rim_z@13	3.65E-07	4.52E-08	1.51E+01	4.07E-01	0.2051	2.44E+04
Day_rim_z@14	2.50E-07	4.81E-08	8.48E+00	6.21E-02	0.1935	2.06E+04
Day_rim_z@15	4.38E-07	6.76E-08	6.93E+00	2.17E-01	0.09196	1.96E+04
Day_rim_z@16	7.50E-07	1.31E-07	4.71E+00	4.32E-02	0.02874	1.91E+04
Day_rim_z@17	2.76E-07	3.54E-08	1.30E+01	1.08E-01	0.1053	1.96E+04

Table 2 continued
Raw data for Dayingshan zircon rims and cores collected from SIMS analyses. 1 s.e. is the standard error, which represents measurement uncertainty. Background is measured at 246.3 and 244.038, respectively.

Sample	*246.02804*	*244.0381*	*248.3*	*254.3*	*U O/*	*U O/*
					235U O	*235U O*
						1 s.e.
Day_rim_z@1	8.462	1.40E+00	4.67E+02	-3.83E+02	1.36E+02	5.03E-01
Day_rim_z@2	4.133	2.64E-01	4.24E+02	-5.91E+02	1.38E+02	1.08E+00
Day_rim_z@3	2.228	1.33E-01	5.31E+02	-1.77E+03	1.35E+02	1.12E+00
Day_rim_z@4	1.799	3.83E-01	1.75E+02	-1.33E+03	1.38E+02	1.06E+00
Day_rim_z@5	3.381	1.50E-01	1.07E+03	-8.85E+02	1.38E+02	1.58E+00
Day_rim_z@6	4.138	3.29E-01	4.21E+02	-1.17E+03	1.39E+02	8.68E-01
Day_rim_z@7	1.87	1.65E-01	2.22E+02	-1.51E+03	1.38E+02	1.79E+00
Day_rim_z@8	3.033	1.71E-01	1.13E+02	-6.65E+02	1.38E+02	7.83E-01
Day_rim_z@9	3.785	2.65E-01	9.52E+02	-1.56E+03	1.16E+02	9.68E-01
Day_rim_z@10	2.418	1.33E-01	4.12E+02	-7.80E+02	1.37E+02	1.17E+00
Day_rim_z@11	2.739	2.58E-01	3.67E+02	-1.01E+03	1.33E+02	9.80E-01
Day_rim_z@12	6.151	4.60E-01	1.34E+02	-1.29E+03	1.39E+02	5.28E-01
Day_rim_z@13	4.824	2.25E-01	7.87E+00	-1.01E+03	1.38E+02	6.41E-01
Day_rim_z@14	2.856	9.27E-02	6.05E+02	-1.03E+03	1.38E+02	1.04E+00
Day_rim_z@15	2.311	1.45E-01	7.62E+02	-1.50E+03	1.36E+02	1.14E+00
Day_rim_z@16	1.563	1.14E-01	4.72E+02	-3.11E+02	1.39E+02	1.56E+00
Day_rim_z@17	4.227	2.10E-01	1.05E+03	-9.74E+02	1.37E+02	6.50E-01

Table 2 continued
Raw data for Dayingshan zircon rims and cores collected from SIMS analyses. 1 s.e. is the standard error, which represents measurement uncertainty. Background is measured at 246.3 and 244.038, respectively.

Sample	*251.03885/*	*251.03885/*	*Bckgr*			
	235U O	*235U O*	*U O*	*U O*	*Th O*	*Th O*
		1 s.e.		**1 s.e.**		**1 s.e.**
Day_rim_z@1	9.63E-01	5.00E-03	1.332E-06	2.33E-07	2.06E-06	3.53E-07
Day_rim_z@2	9.69E-01	6.40E-03	5.848E-07	1.26E-07	3.25E-07	6.90E-08
Day_rim_z@3	9.73E-01	7.75E-03	5.835E-07	2.49E-07	3.73E-07	1.54E-07
Day_rim_z@4	9.88E-01	1.02E-02	1.825E-06	4.63E-07	1.55E-06	3.99E-07
Day_rim_z@5	9.69E-01	7.18E-03	2.449E-07	6.11E-08	2.76E-07	6.90E-08
Day_rim_z@6	9.70E-01	7.76E-03	5.673E-07	1.12E-07	3.34E-07	6.61E-08
Day_rim_z@7	9.87E-01	1.07E-02	1.219E-06	3.14E-07	3.70E-07	9.43E-08
Day_rim_z@8	9.70E-01	7.31E-03	6.031E-07	2.81E-07	3.49E-07	1.50E-07
Day_rim_z@9	9.78E-01	7.14E-03	5.167E-07	1.01E-07	2.54E-07	4.92E-08
Day_rim_z@10	9.83E-01	8.38E-03	4.508E-07	1.23E-07	3.76E-07	1.03E-07
Day_rim_z@11	9.69E-01	1.07E-02	6.553E-07	1.29E-07	6.41E-07	1.26E-07
Day_rim_z@12	9.77E-01	5.42E-03	5.482E-07	9.22E-08	4.19E-07	6.90E-08
Day_rim_z@13	9.68E-01	7.19E-03	3.966E-07	1.22E-07	3.58E-07	1.09E-07
Day_rim_z@14	9.73E-01	8.19E-03	5.497E-07	2.85E-07	3.92E-07	2.03E-07
Day_rim_z@15	9.68E-01	1.11E-02	5.785E-07	2.01E-07	3.73E-07	1.39E-07
Day_rim_z@16	9.80E-01	1.23E-02	5.003E-07	1.61E-07	4.73E-07	1.52E-07
Day_rim_z@17	9.73E-01	7.08E-03	4.053E-07	8.73E-08	2.05E-07	4.38E-08

Table 2 continued
Raw data for Dayingshan zircon rims and cores collected from SIMS analyses. 1 s.e. is the standard error, which represents measurement uncertainty. Background is measured at 246.3 and 244.038, respectively.

	(246.3 only)					
Sample	**246.029/**	**246.029/**	**U O/**	**U O/**	**246.029/**	**246.029/**
	U O	**U O**	**Th O**	**Th O**	**Th O**	**Th O**
		1 s.e.		**1 s.e.**		**1 s.e.**
Day_rim_z@1	1.270E-05	7.347E-07	1.562E+00	5.537E-03	1.976E-05	1.080E-06
Day_rim_z@2	1.034E-05	3.500E-07	5.520E-01	1.030E-02	5.690E-06	1.999E-07
Day_rim_z@3	1.011E-05	5.366E-07	6.545E-01	6.150E-03	6.629E-06	3.431E-07
Day_rim_z@4	1.108E-05	7.958E-07	8.452E-01	5.472E-03	9.324E-06	6.735E-07
Day_rim_z@5	7.845E-06	2.636E-07	1.109E+00	1.860E-02	8.691E-06	2.926E-07
Day_rim_z@6	1.000E-05	3.278E-07	5.916E-01	2.384E-03	5.919E-06	1.939E-07
Day_rim_z@7	1.321E-05	8.719E-07	3.076E-01	4.302E-03	4.102E-06	2.926E-07
Day_rim_z@8	9.807E-06	5.227E-07	6.225E-01	1.925E-02	6.116E-06	3.234E-07
Day_rim_z@9	1.138E-05	3.632E-07	4.941E-01	3.063E-03	5.612E-06	1.791E-07
Day_rim_z@10	8.862E-06	3.791E-07	8.326E-01	1.351E-02	7.406E-06	3.493E-07
Day_rim_z@11	9.830E-06	3.895E-07	9.761E-01	9.083E-03	9.611E-06	3.797E-07
Day_rim_z@12	9.886E-06	2.752E-07	7.689E-01	3.356E-03	7.592E-06	2.018E-07
Day_rim_z@13	8.230E-06	2.962E-07	9.122E-01	6.783E-03	7.490E-06	2.561E-07
Day_rim_z@14	9.848E-06	5.416E-07	7.213E-01	3.745E-03	7.111E-06	3.880E-07
Day_rim_z@15	1.030E-05	5.211E-07	6.304E-01	1.173E-02	6.476E-06	3.560E-07
Day_rim_z@16	1.087E-05	5.502E-07	9.366E-01	7.123E-03	1.015E-05	5.153E-07
Day_rim_z@17	1.055E-05	3.507E-07	5.034E-01	3.414E-03	5.315E-06	1.801E-07

Table 2 continued
Raw data for Dayingshan zircon rims and cores collected from SIMS analyses. 1 s.e. is the standard error, which represents measurement uncertainty. Background is measured at 246.3 and 244.038, respectively.

	(average 246.3 + 244.038)					
Sample	**246.029/**	**246.029/**	**U O/**	**U O/**	**246.029/**	**246.029/**
	U O	**U O**	**Th O**	**Th O**	**Th O**	**Th O**
		1 s.e.		**1 s.e.**		**1 s.e.**
Day_rim_z@1	1.161E-05	7.667E-07	1.562E+00	5.537E-03	1.807E-05	1.129E-06
Day_rim_z@2	1.022E-05	3.364E-07	5.520E-01	1.030E-02	5.620E-06	1.935E-07
Day_rim_z@3	1.006E-05	4.873E-07	6.545E-01	6.150E-03	6.589E-06	3.142E-07
Day_rim_z@4	1.032E-05	7.476E-07	8.452E-01	5.472E-03	8.692E-06	6.268E-07
Day_rim_z@5	7.734E-06	2.620E-07	1.109E+00	1.860E-02	8.566E-06	2.907E-07
Day_rim_z@6	9.773E-06	3.188E-07	5.916E-01	2.384E-03	5.782E-06	1.885E-07
Day_rim_z@7	1.316E-05	8.338E-07	3.076E-01	4.302E-03	4.082E-06	2.826E-07
Day_rim_z@8	9.807E-06	4.493E-07	6.225E-01	1.925E-02	6.104E-06	2.912E-07
Day_rim_z@9	1.108E-05	3.642E-07	4.941E-01	3.063E-03	5.466E-06	1.795E-07
Day_rim_z@10	8.790E-06	3.700E-07	8.326E-01	1.351E-02	7.335E-06	3.438E-07
Day_rim_z@11	9.525E-06	3.838E-07	9.761E-01	9.083E-03	9.307E-06	3.747E-07
Day_rim_z@12	9.612E-06	2.772E-07	7.689E-01	3.356E-03	7.386E-06	2.026E-07
Day_rim_z@13	8.224E-06	2.746E-07	9.122E-01	6.783E-03	7.483E-06	2.362E-07
Day_rim_z@14	1.005E-05	4.655E-07	7.213E-01	3.745E-03	7.253E-06	3.342E-07
Day_rim_z@15	1.018E-05	4.925E-07	6.304E-01	1.173E-02	6.411E-06	3.348E-07
Day_rim_z@16	1.057E-05	5.442E-07	9.366E-01	7.123E-03	9.877E-06	5.094E-07
Day_rim_z@17	1.041E-05	3.468E-07	5.034E-01	3.414E-03	5.243E-06	1.783E-07

Table 2 continued
Raw data for Dayingshan zircon rims and cores collected from SIMS analyses. 1 s.e. is the standard error, which represents measurement uncertainty. Background is measured at 246.3 and 244.038, respectively.

	gain corrected (average gain 1.005E+00)					
Sample	**246.029/**	**246.029/**	**U O/**	**U O/**	**246.029/**	**246.029/**
	U O	**U O**	**Th O**	**Th O**	**Th O**	**Th O**
		1 s.e.		**1 s.e.**		**1 s.e.**
Day_rim_z@1	1.166E-05	7.704E-07	1.562E+00	5.537E-03	1.815E-05	1.135E-06
Day_rim_z@2	1.026E-05	3.380E-07	5.520E-01	1.030E-02	5.647E-06	1.944E-07
Day_rim_z@3	1.010E-05	4.896E-07	6.545E-01	6.150E-03	6.620E-06	3.157E-07
Day_rim_z@4	1.036E-05	7.512E-07	8.452E-01	5.472E-03	8.733E-06	6.298E-07
Day_rim_z@5	7.771E-06	2.633E-07	1.109E+00	1.860E-02	8.607E-06	2.921E-07
Day_rim_z@6	9.819E-06	3.204E-07	5.916E-01	2.384E-03	5.809E-06	1.894E-07
Day_rim_z@7	1.322E-05	8.378E-07	3.076E-01	4.302E-03	4.102E-06	2.840E-07
Day_rim_z@8	9.854E-06	4.514E-07	6.225E-01	1.925E-02	6.133E-06	2.926E-07
Day_rim_z@9	1.114E-05	3.660E-07	4.941E-01	3.063E-03	5.492E-06	1.803E-07
Day_rim_z@10	8.832E-06	3.718E-07	8.326E-01	1.351E-02	7.370E-06	3.455E-07
Day_rim_z@11	9.570E-06	3.856E-07	9.761E-01	9.083E-03	9.352E-06	3.764E-07
Day_rim_z@12	9.658E-06	2.785E-07	7.689E-01	3.356E-03	7.421E-06	2.036E-07
Day_rim_z@13	8.264E-06	2.759E-07	9.122E-01	6.783E-03	7.519E-06	2.373E-07
Day_rim_z@14	1.010E-05	4.677E-07	7.213E-01	3.745E-03	7.288E-06	3.358E-07
Day_rim_z@15	1.023E-05	4.948E-07	6.304E-01	1.173E-02	6.441E-06	3.364E-07
Day_rim_z@16	1.062E-05	5.467E-07	9.366E-01	7.123E-03	9.924E-06	5.118E-07
Day_rim_z@17	1.046E-05	3.484E-07	5.034E-01	3.414E-03	5.268E-06	1.791E-07

Table 2 continued
Raw data for Dayingshan zircon rims and cores collected from SIMS analyses. 1 s.e. is the standard error, which represents measurement uncertainty. Background is measured at 246.3 and 244.038, respectively.

Sample	*246.02804/*	*246.02804/*	*U O/*	*U O/*	*246.02804/*	*246.02804/*
	U O	*U O*	*Th O*	*Th O*	*Th O*	*Th O*
		1 s.e.		**1 s.e.**		**1 s.e.**
Day_int_z@1	8.85E-06	1.51E-07	1.46E+00	1.15E-02	1.29E-05	2.44E-07
Day_int_z@2	1.02E-05	3.65E-07	6.57E-01	1.18E-02	6.69E-06	2.40E-07
Day_int_z@3	8.82E-06	3.82E-07	5.97E-01	6.11E-03	5.27E-06	2.29E-07
Day_int_z@4	1.07E-05	4.21E-07	5.51E-01	6.95E-03	5.91E-06	2.32E-07
Day_int_z@5	1.01E-05	4.46E-07	5.40E-01	1.91E-02	5.39E-06	2.37E-07
Day_int_z@6	1.10E-05	3.40E-07	4.90E-01	4.03E-03	5.40E-06	1.67E-07
Day_int_z@7	1.29E-05	5.52E-07	2.70E-01	2.44E-03	3.46E-06	1.49E-07
Day_int_z@8	1.15E-05	4.90E-07	3.56E-01	2.87E-03	4.07E-06	1.74E-07
Day_int_z@9	1.34E-05	3.86E-07	3.22E-01	2.58E-03	4.30E-06	1.20E-07
Day_int_z@10	1.06E-05	3.83E-07	5.96E-01	8.19E-03	6.36E-06	2.75E-07
Day_int_z@11	9.47E-06	2.67E-07	6.13E-01	6.41E-03	5.80E-06	1.64E-07
Day_int_z@12	9.52E-06	1.95E-07	7.15E-01	1.73E-03	6.80E-06	1.39E-07
Day_int_z@13	9.39E-06	3.21E-07	6.65E-01	8.85E-03	6.23E-06	2.13E-07
Day_int_z@14	1.13E-05	1.40E-06	6.42E-01	5.40E-03	7.27E-06	9.34E-07
Day_int_z@15	1.02E-05	3.90E-07	5.83E-01	4.59E-03	5.96E-06	2.28E-07
Day_int_z@16	1.40E-05	5.88E-07	1.50E+00	2.33E-02	2.09E-05	9.09E-07
Day_int_z@17	1.02E-05	3.32E-07	5.27E-01	6.04E-03	5.38E-06	1.75E-07
Day_int_z@18	8.05E-06	4.61E-07	1.49E+00	1.59E-02	1.19E-05	6.83E-07
Day_int_z@19	1.11E-05	3.80E-07	4.63E-01	1.70E-03	5.15E-06	1.76E-07
Day_int_z@21	9.26E-06	2.12E-07	6.33E-01	2.66E-03	5.86E-06	1.34E-07
Day_int_z@22	1.03E-05	3.02E-07	5.63E-01	9.44E-03	5.83E-06	2.13E-07
Day_int_z@23	1.03E-05	3.52E-07	4.59E-01	1.73E-03	4.73E-06	1.62E-07

Table 2 continued
Raw data for Dayingshan zircon rims and cores collected from SIMS analyses. 1 s.e. is the standard error, which represents measurement uncertainty. Background is measured at 246.3 and 244.038, respectively.

Sample	*246.3/*	*246.3/*	*246.3/*	*246.3/*	*244.0381/*	*244.0381/*
	U O	*U O*	*Th O*	*Th O*	*U O*	*U O*
		1 s.e.		**1 s.e.**		**1 s.e.**
Day_int_z@1	2.35E-08	1.58E-08	3.37E-08	2.26E-08	1.31E-07	1.91E-08
Day_int_z@2	7.50E-08	6.82E-08	4.67E-08	4.21E-08	4.27E-07	7.53E-08
Day_int_z@3	1.09E-07	8.37E-08	6.82E-08	5.21E-08	7.95E-07	1.15E-07
Day_int_z@4	3.41E-07	1.96E-07	1.90E-07	1.13E-07	5.42E-07	9.47E-08
Day_int_z@5	2.59E-07	1.47E-07	1.43E-07	8.28E-08	9.93E-07	1.58E-07
Day_int_z@6	2.44E-07	1.08E-07	1.20E-07	5.38E-08	3.18E-07	5.82E-08
Day_int_z@7	7.22E-07	2.76E-07	1.93E-07	7.42E-08	1.02E-06	1.56E-07
Day_int_z@8	2.58E-07	1.36E-07	9.28E-08	4.87E-08	8.29E-07	1.39E-07
Day_int_z@9	4.29E-07	1.76E-07	1.38E-07	5.79E-08	8.75E-07	9.34E-08
Day_int_z@10	3.99E-07	1.93E-07	2.36E-07	1.17E-07	5.34E-07	7.70E-08
Day_int_z@11	3.55E-07	1.04E-07	2.15E-07	6.30E-08	3.48E-07	5.18E-08
Day_int_z@12	1.06E-07	4.44E-08	7.57E-08	3.17E-08	2.47E-07	3.14E-08
Day_int_z@13	3.12E-07	1.12E-07	2.13E-07	7.72E-08	5.11E-07	7.39E-08
Day_int_z@14	1.96E-07	1.14E-07	1.24E-07	7.25E-08	4.41E-07	7.05E-08
Day_int_z@15	5.62E-07	1.82E-07	3.22E-07	1.04E-07	4.60E-07	8.31E-08
Day_int_z@16	2.44E-07	1.63E-07	3.71E-07	2.47E-07	8.18E-07	1.43E-07
Day_int_z@17	2.57E-07	1.15E-07	1.32E-07	5.85E-08	4.62E-07	7.13E-08
Day_int_z@18	6.52E-07	2.89E-07	1.01E-06	4.46E-07	7.06E-07	1.36E-07
Day_int_z@19	3.43E-07	1.23E-07	1.58E-07	5.65E-08	4.57E-07	7.72E-08
Day_int_z@21	1.26E-07	5.58E-08	7.90E-08	3.47E-08	3.22E-07	3.95E-08
Day_int_z@22	5.88E-08	4.90E-08	3.34E-08	2.83E-08	9.84E-07	9.34E-08
Day_int_z@23	4.36E-07	1.69E-07	1.99E-07	7.74E-08	2.07E-06	1.58E-07

Table 2 continued
Raw data for Dayingshan zircon rims and cores collected from SIMS analyses. 1 s.e. is the standard error, which represents measurement uncertainty. Background is measured at 246.3 and 244.038, respectively.

Sample	*244.0381/*	*244.0381/*	*U O/*	*U O/*	*246.3*	*92Zr Zr O4*
	Th O	*Th O*	*Zr2 O4*	*Zr2 O4*		
		1 s.e.		**1 s.e.**		
Day_int_z@1	1.90E-07	2.72E-08	3.79E+01	1.32E+00	0.03445	2.34E+04
Day_int_z@2	2.86E-07	5.04E-08	7.59E+00	1.55E-01	0.02107	2.22E+04
Day_int_z@3	4.77E-07	6.89E-08	5.66E+00	3.86E-02	0.02298	2.40E+04
Day_int_z@4	2.96E-07	5.18E-08	6.17E+00	2.00E-01	0.06895	2.13E+04
Day_int_z@5	4.94E-07	7.07E-08	5.28E+00	9.73E-02	0.04597	2.12E+04
Day_int_z@6	1.57E-07	2.87E-08	9.76E+00	3.66E-01	0.07088	2.13E+04
Day_int_z@7	2.79E-07	4.27E-08	5.07E+00	8.96E-02	0.1034	1.79E+04
Day_int_z@8	2.98E-07	5.12E-08	5.69E+00	6.42E-02	0.04598	1.98E+04
Day_int_z@9	2.83E-07	3.02E-08	1.10E+01	2.36E-01	0.1494	1.89E+04
Day_int_z@10	3.20E-07	4.62E-08	7.15E+00	4.16E-01	0.134	2.66E+04
Day_int_z@11	2.13E-07	3.18E-08	1.08E+01	1.88E-01	0.1609	2.75E+04
Day_int_z@12	1.77E-07	2.25E-08	1.97E+01	7.08E-02	0.09193	2.87E+04
Day_int_z@13	3.33E-07	4.81E-08	7.29E+00	2.96E-01	0.09196	2.66E+04
Day_int_z@14	2.80E-07	4.49E-08	7.11E+00	4.81E-02	0.05755	2.76E+04
Day_int_z@15	2.67E-07	4.83E-08	5.66E+00	1.12E-01	0.1284	2.66E+04
Day_int_z@16	1.21E-06	2.12E-07	3.31E+00	2.62E-02	0.03452	2.69E+04
Day_int_z@17	2.44E-07	3.77E-08	7.31E+00	1.41E-01	0.08049	2.81E+04
Day_int_z@18	1.06E-06	2.04E-07	3.81E+00	3.65E-02	0.09002	2.35E+04
Day_int_z@19	2.11E-07	3.56E-08	7.27E+00	3.55E-02	0.09	2.46E+04
Day_int_z@21	2.03E-07	2.49E-08	1.77E+01	3.11E-01	0.08814	2.05E+04
Day_int_z@22	5.46E-07	5.12E-08	1.00E+01	2.49E-01	0.02299	2.84E+04
Day_int_z@23	9.50E-07	7.25E-08	5.81E+00	9.53E-02	0.1245	3.90E+04

Table 2 continued
Raw data for Dayingshan zircon rims and cores collected from SIMS analyses. 1 s.e. is the standard error, which represents measurement uncertainty. Background is measured at 246.3 and 244.038, respectively.

Sample	*246.02804*	*244.0381*	*248.3*	*254.3*	*U O/*	*U O/*
					235U O	*235U O*
						1 s.e.
Day_int_z@1	11.84	1.80E-01	7.98E+02	-1.26E+03	1.37E+02	4.52E-01
Day_int_z@2	2.691	1.11E-01	3.11E+02	-1.90E+03	1.39E+02	1.01E+00
Day_int_z@3	1.837	1.65E-01	3.27E+02	-1.57E+03	1.39E+02	1.17E+00
Day_int_z@4	2.244	1.13E-01	3.76E+02	-1.42E+03	1.37E+02	9.09E-01
Day_int_z@5	1.78	1.69E-01	-2.12E+01	-1.27E+03	1.38E+02	1.45E+00
Day_int_z@6	3.619	1.03E-01	4.35E+02	-6.05E+02	1.31E+02	8.22E-01
Day_int_z@7	1.867	1.47E-01	-2.61E+02	-1.75E+03	1.41E+02	1.52E+00
Day_int_z@8	1.882	1.36E-01	-4.98E+02	-1.40E+03	1.35E+02	1.29E+00
Day_int_z@9	4.656	3.02E-01	4.84E+02	-1.14E+03	7.67E+01	8.41E-01
Day_int_z@10	3.386	1.66E-01	3.18E+02	-1.44E+03	1.30E+02	1.41E+00
Day_int_z@11	4.323	1.56E-01	3.44E+02	-2.23E+03	1.38E+02	6.86E-01
Day_int_z@12	8.214	2.13E-01	-4.16E+02	-1.82E+03	1.38E+02	4.75E-01
Day_int_z@13	2.946	1.65E-01	-7.12E+01	-2.59E+03	1.32E+02	9.60E-01
Day_int_z@14	3.432	1.35E-01	-3.35E+02	-2.09E+03	1.38E+02	9.82E-01
Day_int_z@15	2.377	1.06E-01	4.60E+02	-1.99E+03	1.38E+02	1.05E+00
Day_int_z@16	1.939	1.13E-01	4.34E+01	-2.20E+03	1.37E+02	1.66E+00
Day_int_z@17	3.281	1.44E-01	3.14E+02	-3.00E+03	1.37E+02	7.96E-01
Day_int_z@18	1.051	9.31E-02	7.10E+02	-1.88E+03	1.40E+02	1.81E+00
Day_int_z@19	2.956	1.21E-01	9.62E+02	-1.65E+03	1.39E+02	9.44E-01
Day_int_z@21	6.606	2.29E-01	5.36E+02	-1.77E+03	1.39E+02	6.31E-01
Day_int_z@22	4.023	3.92E-01	-2.60E+02	-2.19E+03	1.18E+02	1.33E+00
Day_int_z@23	2.941	5.92E-01	5.34E+02	-1.84E+03	1.39E+02	8.31E-01

Table 2 continued
Raw data for Dayingshan zircon rims and cores collected from SIMS analyses. 1 s.e. is the standard error, which represents measurement uncertainty. Background is measured at 246.3 and 244.038, respectively.

Sample	*251.03885/*	*251.03885/*	*Bckgr*			
	235U O	*235U O*	*U O*	*U O*	*Th O*	*Th O*
		1 s.e.				
Day_int_z@1	9.74E-01	4.11E-03	7.732E-08	1.75E-08	1.12E-07	2.50E-08
Day_int_z@2	9.80E-01	7.44E-03	2.510E-07	7.18E-08	1.66E-07	4.65E-08
Day_int_z@3	9.63E-01	7.51E-03	4.518E-07	1.00E-07	2.72E-07	6.11E-08
Day_int_z@4	9.86E-01	8.98E-03	4.417E-07	1.54E-07	2.43E-07	8.80E-08
Day_int_z@5	9.84E-01	1.45E-02	6.262E-07	1.52E-07	3.19E-07	7.70E-08
Day_int_z@6	9.81E-01	7.23E-03	2.808E-07	8.64E-08	1.39E-07	4.31E-08
Day_int_z@7	9.92E-01	1.32E-02	8.692E-07	2.24E-07	2.36E-07	6.05E-08
Day_int_z@8	9.68E-01	8.82E-03	5.435E-07	1.38E-07	1.95E-07	5.00E-08
Day_int_z@9	9.74E-01	5.79E-03	6.521E-07	1.41E-07	2.10E-07	4.62E-08
Day_int_z@10	9.76E-01	7.32E-03	4.666E-07	1.47E-07	2.78E-07	8.92E-08
Day_int_z@11	9.77E-01	7.69E-03	3.514E-07	8.19E-08	2.14E-07	4.99E-08
Day_int_z@12	9.74E-01	4.85E-03	1.764E-07	3.84E-08	1.26E-07	2.75E-08
Day_int_z@13	9.64E-01	9.39E-03	4.115E-07	9.47E-08	2.73E-07	6.43E-08
Day_int_z@14	9.74E-01	8.94E-03	3.185E-07	9.46E-08	2.02E-07	6.03E-08
Day_int_z@15	9.78E-01	9.07E-03	5.107E-07	1.41E-07	2.95E-07	8.12E-08
Day_int_z@16	9.64E-01	1.45E-02	5.310E-07	1.53E-07	7.92E-07	2.30E-07
Day_int_z@17	9.73E-01	7.17E-03	3.595E-07	9.57E-08	1.88E-07	4.92E-08
Day_int_z@18	9.77E-01	1.15E-02	6.790E-07	2.26E-07	1.03E-06	3.47E-07
Day_int_z@19	9.72E-01	8.17E-03	4.000E-07	1.02E-07	1.84E-07	4.72E-08
Day_int_z@21	9.73E-01	6.80E-03	2.240E-07	4.84E-08	1.41E-07	3.02E-08
Day_int_z@22	9.74E-01	7.60E-03	5.213E-07	7.46E-08	2.90E-07	4.14E-08
Day_int_z@23	9.87E-01	7.67E-03	1.251E-06	1.63E-07	5.75E-07	7.50E-08

Table 2 continued
Raw data for Dayingshan zircon rims and cores collected from SIMS analyses. 1 s.e. is the standard error, which represents measurement uncertainty. Background is measured at 246.3 and 244.038, respectively.

	(246.3 only)					
Sample	**246.029/**	**246.029/**	**U O/**	**U O/**	**246.029/**	**246.029/**
	U O	**U O**	**Th O**	**Th O**	**Th O**	**Th O**
		1 s.e.		**1 s.e.**		**1 s.e.**
Day_int_z@1	8.827E-06	1.519E-07	1.459E+00	1.145E-02	1.290E-05	2.447E-07
Day_int_z@2	1.014E-05	3.717E-07	6.572E-01	1.177E-02	6.646E-06	2.433E-07
Day_int_z@3	8.715E-06	3.913E-07	5.972E-01	6.114E-03	5.206E-06	2.344E-07
Day_int_z@4	1.040E-05	4.645E-07	5.508E-01	6.946E-03	5.723E-06	2.580E-07
Day_int_z@5	9.881E-06	4.699E-07	5.400E-01	1.913E-02	5.244E-06	2.511E-07
Day_int_z@6	1.078E-05	3.567E-07	4.902E-01	4.032E-03	5.282E-06	1.752E-07
Day_int_z@7	1.213E-05	6.174E-07	2.695E-01	2.441E-03	3.262E-06	1.660E-07
Day_int_z@8	1.119E-05	5.085E-07	3.559E-01	2.866E-03	3.975E-06	1.808E-07
Day_int_z@9	1.295E-05	4.243E-07	3.221E-01	2.578E-03	4.163E-06	1.331E-07
Day_int_z@10	1.022E-05	4.283E-07	5.962E-01	8.188E-03	6.125E-06	2.989E-07
Day_int_z@11	9.112E-06	2.868E-07	6.128E-01	6.411E-03	5.583E-06	1.754E-07
Day_int_z@12	9.411E-06	2.000E-07	7.149E-01	1.731E-03	6.726E-06	1.430E-07
Day_int_z@13	9.082E-06	3.403E-07	6.649E-01	8.849E-03	6.014E-06	2.265E-07
Day_int_z@14	1.106E-05	1.400E-06	6.419E-01	5.399E-03	7.143E-06	9.365E-07
Day_int_z@15	9.669E-06	4.301E-07	5.826E-01	4.588E-03	5.641E-06	2.510E-07
Day_int_z@16	1.371E-05	6.104E-07	1.496E+00	2.331E-02	2.051E-05	9.423E-07
Day_int_z@17	9.983E-06	3.514E-07	5.266E-01	6.035E-03	5.252E-06	1.847E-07
Day_int_z@18	7.393E-06	5.438E-07	1.489E+00	1.588E-02	1.091E-05	8.153E-07
Day_int_z@19	1.080E-05	3.996E-07	4.625E-01	1.696E-03	4.993E-06	1.847E-07
Day_int_z@21	9.129E-06	2.187E-07	6.327E-01	2.662E-03	5.781E-06	1.383E-07
Day_int_z@22	1.026E-05	3.063E-07	5.629E-01	9.438E-03	5.797E-06	2.150E-07
Day_int_z@23	9.854E-06	3.905E-07	4.594E-01	1.733E-03	4.528E-06	1.795E-07

Table 2 continued
Raw data for Dayingshan zircon rims and cores collected from SIMS analyses. 1 s.e. is the standard error, which represents measurement uncertainty. Background is measured at 246.3 and 244.038, respectively.

	(average 246.3 + 244.038)					
Sample	**246.029/**	**246.029/**	**U O/**	**U O/**	**246.029/**	**246.029/**
	U O	**U O**	**Th O**	**Th O**	**Th O**	**Th O**
		1 s.e.		**1 s.e.**		**1 s.e.**
Day_int_z@1	8.774E-06	1.521E-07	1.459E+00	1.145E-02	1.282E-05	2.450E-07
Day_int_z@2	9.959E-06	3.724E-07	6.572E-01	1.177E-02	6.527E-06	2.441E-07
Day_int_z@3	8.372E-06	3.953E-07	5.972E-01	6.114E-03	5.002E-06	2.365E-07
Day_int_z@4	1.030E-05	4.484E-07	5.508E-01	6.946E-03	5.670E-06	2.480E-07
Day_int_z@5	9.514E-06	4.717E-07	5.400E-01	1.913E-02	5.068E-06	2.493E-07
Day_int_z@6	1.074E-05	3.509E-07	4.902E-01	4.032E-03	5.264E-06	1.722E-07
Day_int_z@7	1.198E-05	5.960E-07	2.695E-01	2.441E-03	3.219E-06	1.604E-07
Day_int_z@8	1.091E-05	5.090E-07	3.559E-01	2.866E-03	3.873E-06	1.811E-07
Day_int_z@9	1.273E-05	4.110E-07	3.221E-01	2.578E-03	4.091E-06	1.285E-07
Day_int_z@10	1.015E-05	4.098E-07	5.962E-01	8.188E-03	6.083E-06	2.890E-07
Day_int_z@11	9.116E-06	2.797E-07	6.128E-01	6.411E-03	5.584E-06	1.711E-07
Day_int_z@12	9.341E-06	1.988E-07	7.149E-01	1.731E-03	6.676E-06	1.421E-07
Day_int_z@13	8.983E-06	3.351E-07	6.649E-01	8.849E-03	5.954E-06	2.225E-07
Day_int_z@14	1.094E-05	1.398E-06	6.419E-01	5.399E-03	7.065E-06	9.356E-07
Day_int_z@15	9.719E-06	4.146E-07	5.826E-01	4.588E-03	5.668E-06	2.424E-07
Day_int_z@16	1.342E-05	6.079E-07	1.496E+00	2.331E-02	2.009E-05	9.380E-07
Day_int_z@17	9.881E-06	3.456E-07	5.266E-01	6.035E-03	5.196E-06	1.820E-07
Day_int_z@18	7.366E-06	5.131E-07	1.489E+00	1.588E-02	1.089E-05	7.655E-07
Day_int_z@19	1.074E-05	3.939E-07	4.625E-01	1.696E-03	4.967E-06	1.821E-07
Day_int_z@21	9.031E-06	2.170E-07	6.327E-01	2.662E-03	5.719E-06	1.373E-07
Day_int_z@22	9.799E-06	3.114E-07	5.629E-01	9.438E-03	5.540E-06	2.171E-07
Day_int_z@23	9.039E-06	3.883E-07	4.594E-01	1.733E-03	4.152E-06	1.784E-07

Table 2 continued
Raw data for Dayingshan zircon rims and cores collected from SIMS analyses. 1 s.e. is the standard error, which represents measurement uncertainty. Background is measured at 246.3 and 244.038, respectively.

	gain corrected (average gain 1.005E+00)					
Sample	**246.029/**	**246.029/**	**U O/**	**U O/**	**246.029/**	**246.029/**
	U O	**U O**	**Th O**	**Th O**	**Th O**	**Th O**
		1 s.e.		**1 s.e.**		**1 s.e.**
Day_int_z@1	8.816E-06	1.528E-07	1.459E+00	1.145E-02	1.288E-05	2.462E-07
Day_int_z@2	1.001E-05	3.742E-07	6.572E-01	1.177E-02	6.558E-06	2.452E-07
Day_int_z@3	8.412E-06	3.972E-07	5.972E-01	6.114E-03	5.026E-06	2.376E-07
Day_int_z@4	1.035E-05	4.505E-07	5.508E-01	6.946E-03	5.697E-06	2.491E-07
Day_int_z@5	9.559E-06	4.739E-07	5.400E-01	1.913E-02	5.092E-06	2.505E-07
Day_int_z@6	1.079E-05	3.526E-07	4.902E-01	4.032E-03	5.289E-06	1.730E-07
Day_int_z@7	1.204E-05	5.989E-07	2.695E-01	2.441E-03	3.235E-06	1.611E-07
Day_int_z@8	1.096E-05	5.114E-07	3.559E-01	2.866E-03	3.891E-06	1.820E-07
Day_int_z@9	1.279E-05	4.129E-07	3.221E-01	2.578E-03	4.110E-06	1.291E-07
Day_int_z@10	1.020E-05	4.117E-07	5.962E-01	8.188E-03	6.112E-06	2.904E-07
Day_int_z@11	9.159E-06	2.810E-07	6.128E-01	6.411E-03	5.610E-06	1.719E-07
Day_int_z@12	9.385E-06	1.997E-07	7.149E-01	1.731E-03	6.708E-06	1.428E-07
Day_int_z@13	9.025E-06	3.367E-07	6.649E-01	8.849E-03	5.982E-06	2.236E-07
Day_int_z@14	1.099E-05	1.405E-06	6.419E-01	5.399E-03	7.099E-06	9.401E-07
Day_int_z@15	9.766E-06	4.166E-07	5.826E-01	4.588E-03	5.695E-06	2.436E-07
Day_int_z@16	1.348E-05	6.108E-07	1.496E+00	2.331E-02	2.018E-05	9.424E-07
Day_int_z@17	9.928E-06	3.473E-07	5.266E-01	6.035E-03	5.221E-06	1.828E-07
Day_int_z@18	7.401E-06	5.155E-07	1.489E+00	1.588E-02	1.094E-05	7.691E-07
Day_int_z@19	1.079E-05	3.958E-07	4.625E-01	1.696E-03	4.990E-06	1.830E-07
Day_int_z@21	9.074E-06	2.180E-07	6.327E-01	2.662E-03	5.746E-06	1.379E-07
Day_int_z@22	9.845E-06	3.129E-07	5.629E-01	9.438E-03	5.567E-06	2.181E-07
Day_int_z@23	9.082E-06	3.901E-07	4.594E-01	1.733E-03	4.172E-06	1.793E-07

a concentrated beam. The ion beam then travels through the primary ion column before contacting the target sample. Upon contact, a small percentage of target atoms become ionized (typically < 10%) (Stern, 2009). These secondary ions then pass through the secondary ion column into a mass spectrometer containing an electrostatic analyzer (ESA) and an electromagnet. The ESA is used to deflect ions based on their energy levels, while the electromagnet deflects particles based on their masses. Both instruments serve the purpose of increasing the mass resolution. Entrance and exit slits are located before and after the analyzers, and are adjusted accordingly in order to obtain the highest mass resolution. The last step is to measure and count the secondary ions. Several different secondary ion detection measures may be used according to need. These include an ion counting electron multiplier, Faraday cups, and ion image detectors. Figure 13 is a simplified diagram showing these fundamental components of SIMS.

Individual spots on zircons are targeted using Customizable Ion Probe Software (CIPS). Each component of SIMS is monitored and adjusted using CIPS. Individual spots can be targeted by hand due to a magnified view of zircon surfaces in reflected light. The Cameca ims 1270 is also able to image ions, which is useful for targeting specific regions of the sample based on composition. After selecting the placement of each spot, the zircons are sputtered in series, with each zircon taking ~20 minutes to analyze. Once the sputtering process is complete, the data obtained is transferred into a Microsoft Excel spreadsheet. An Excel spreadsheet is necessary in order to use the program Isoplot (Ludwig, 2003), which provides the capability to plot radiogenic isotope data. An Excel spreadsheet also presents the data in a more reader-friendly format, allowing for easier data interpretation.

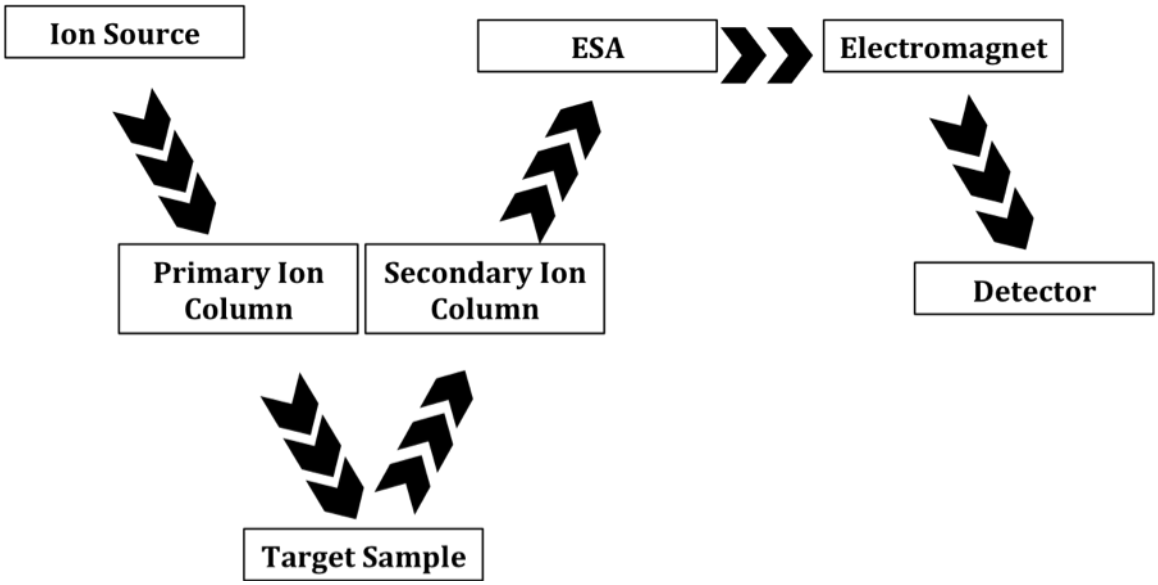

Fig. 13. Diagram depicting the fundamental components of a SIMS instrument (After Stern, 2009).

Erroneous data may be recorded from SIMS due to counting errors, relative sensitivity factor (RSF) uncertainties, primary beam instabilities, zircon surface topography, or changes in surface conductivity with depth (Schmitt, 2009). RSF involves the measuring of faint isotopes adjacent to abundant ones. Systematic errors such as matrix effects, drift in detector gain, and detector non-linearity may also occur (Schmitt, 2009). These problems can typically be held in check by periodically measuring standards while measurements for zircons of unknown age are being made, and by closely monitoring SIMS instrumentation from the control console. Significant Th-U fractionation is absent in zircon, and therefore is not a factor. The most prevalent error in Quaternary zircon measurements is counting errors due to low signals (Schmitt, 2009). Great care was taken to ensure that these errors did not occur.

RESULTS

Dayingshan Whole-Rock Major and Trace Element Analysis

Whole-rock analysis of rock sample YTC9724-5 from Dayingshan (Zou, 2010) yielded similar results to data from Maanshan volcano (Fig. 2) (Zou et al., 2010). The major and trace element concentrations can be seen in Table 3. Of particular interest is the high Zr concentration of 303 ppm. High Zr concentrations indicate a more silicic magma. It is also important to note that SiO_2, FeO and MgO weight percentages of the Dayingshan sample are indicative of a calc-alkaline suite. These concentrations, along with those from several other rocks collected from Dayingshan (Zou, 2010; Wang, F. et al., 2006; Zhao and Fan, 2010) were plotted on a FeO/MgO vs. SiO_2 plot, and demonstrate an overall calc-alkaline trend (Fig. 14).

Calc-alkaline rocks typically show enrichment in silica and alkalies, low enrichment in iron, and typify subduction zones. YTC9724-5 whole-rock analysis also yielded high K. High-K calc-alkaline rocks tend to develop on increasingly thicker continental crust (Best, 2003).

Calc-alkaline rocks are typically enriched in light rare earth elements (LREE's), and show a negative slope on an REE plot (Fig. 15). Plotted trace element patterns in calc-alkaline rocks are commonly irregular, and show enrichment in the more incompatible elements, such as Rb, and depletion in elements with high field strengths, such as Nb and Ta (Best, 2003). Figure 16 is a spider diagram from the

Table 3
Major and trace element concentrations from Dayingshan whole-rock analysis of sample YTC9724-5.

	wt%		ppm		ppm		ppm
SiO2	62.24	La	79.22	Er	3.00	U	3.32
TiO2	0.93	Ce	151.4	Tm	0.43	Pb	25.57
Al2O3	16.01	Pr	16.37	Yb	2.60	Rb	150.3
FeO*	5.45	Nd	57.19	Lu	0.40	Cs	2.02
MnO	0.09	Sm	9.79	Ba	865	Sr	445
MgO	2.35	Eu	1.82	Th	34.32	Sc	10.9
CaO	4.30	Gd	7.40	Nb	27.60	Zr	303
Na2O	3.29	Tb	1.08	Y	29.27		

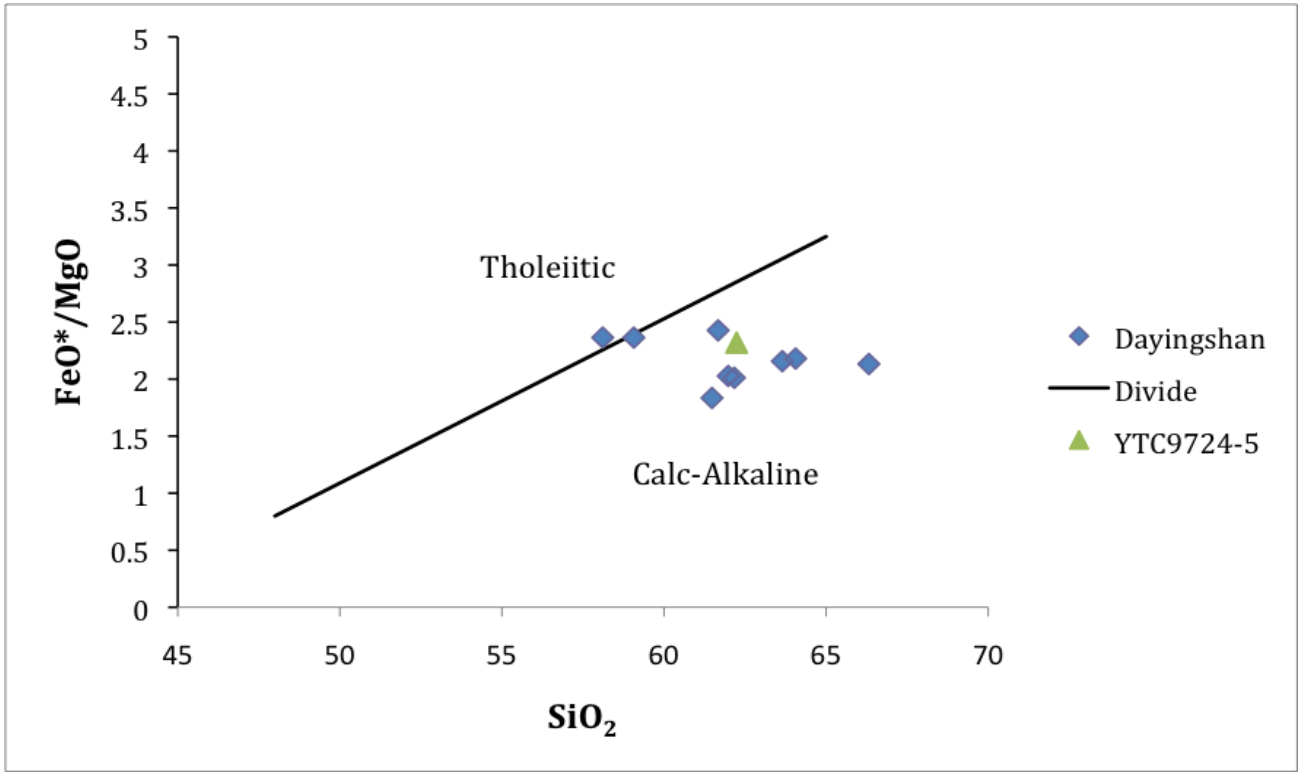

Fig. 14. FeO/MgO vs. SiO_2 plot demonstrating an overall calc-alkaline trend in Dayingshan samples. The dividing line is defined by Irvine and Barager (1971). Data points were collected from Zou (2010), Wang, F. et al. (2006), and Zhao and Fan (2010).

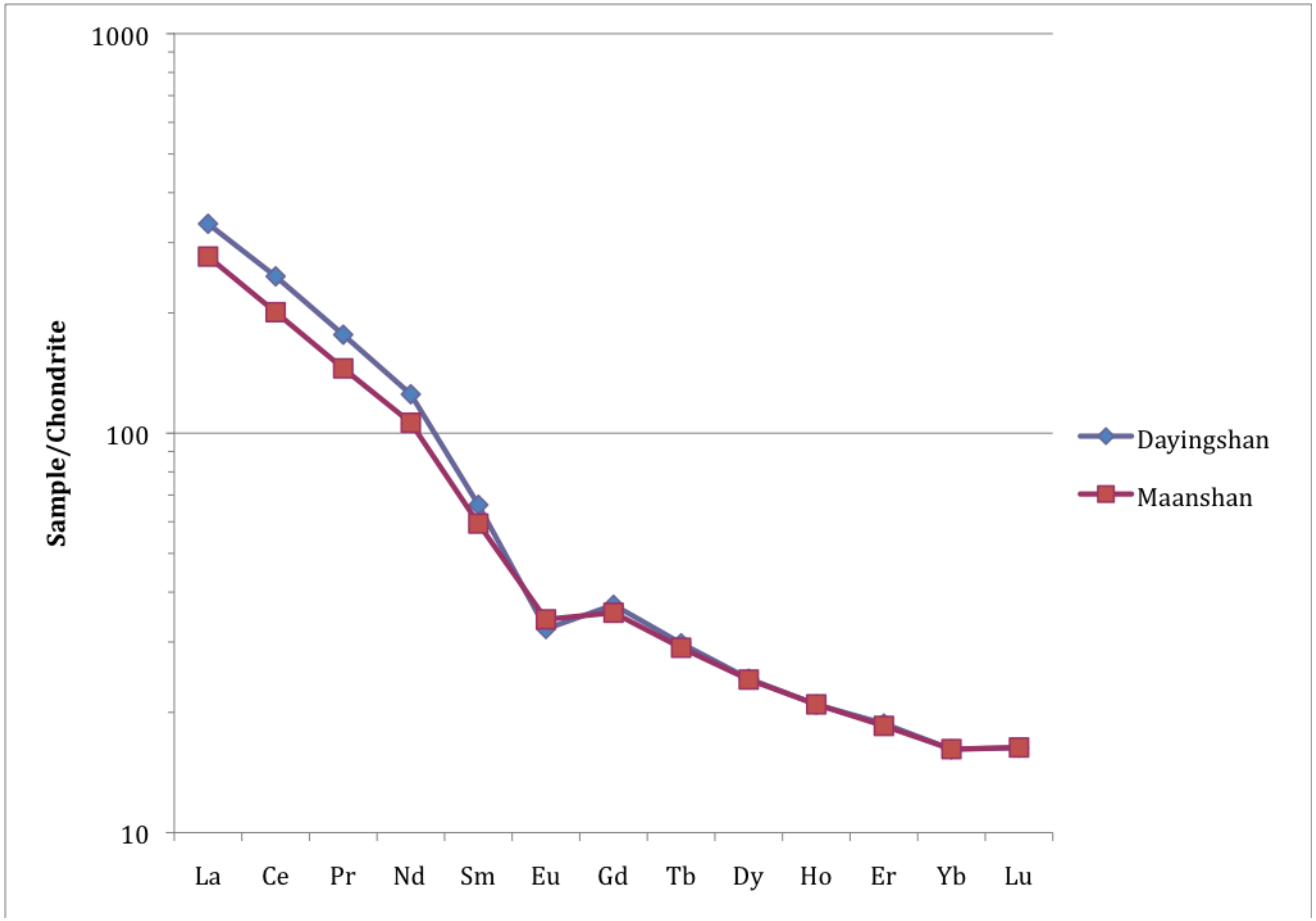

Fig. 15. REE plot of sample YTC9724-5 from Dayingshan and sample MA02 from Maanshan (Zou et al., 2010). The vertical axis is normalized using average abundances in chondritic meteorites. The negative slope indicates enrichment in LREE's.

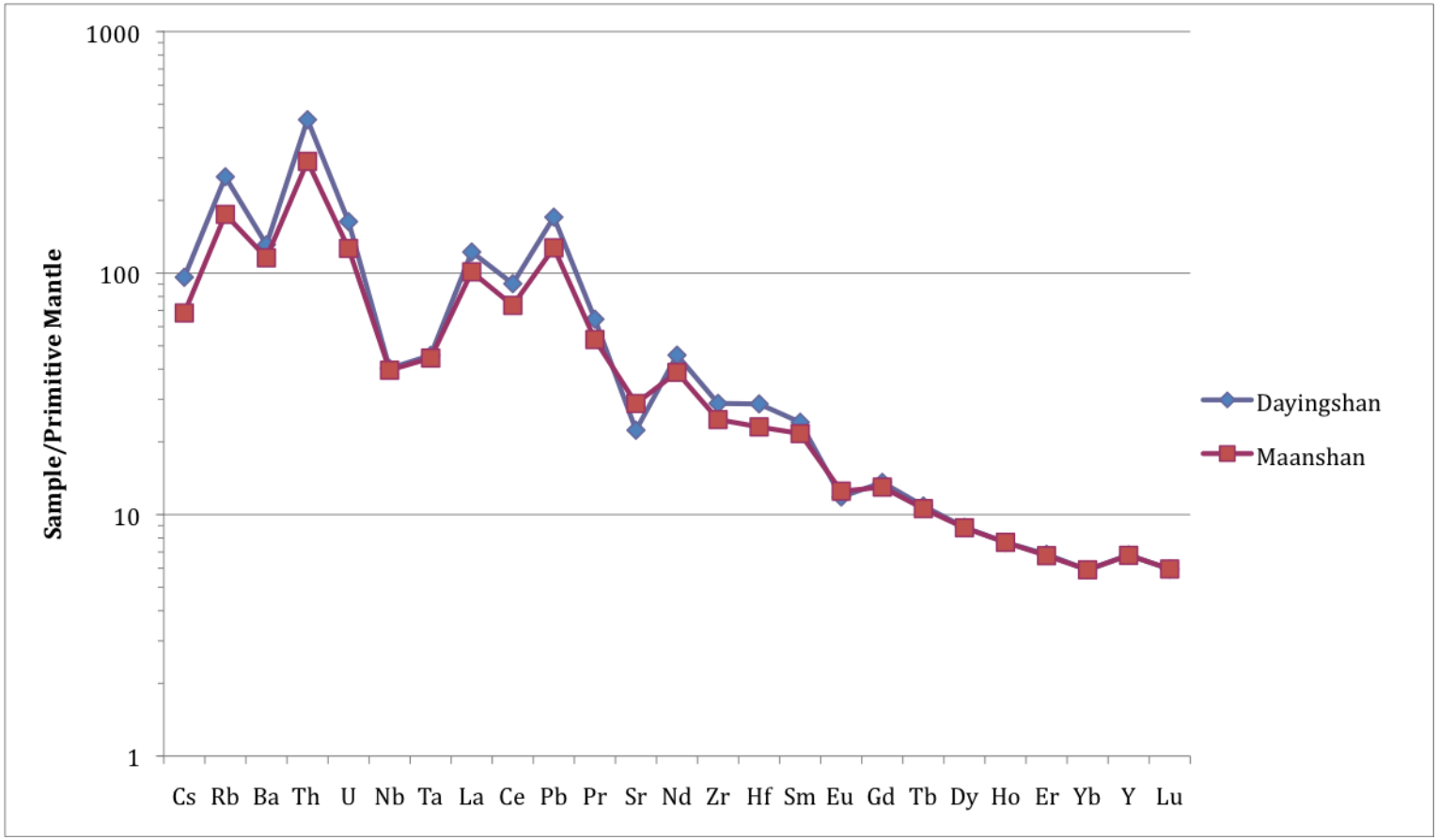

Fig. 16. Spider diagram of Dayingshan (YTC9724-5) and Maanshan (MA02) (Zou et al., 2010) trace elements. The vertical axis is normalized using estimated primitive mantle. A spiked, irregular pattern with an overall negative slope is indicative of a calc-alkaline sample.

Dayingshan sample, which demonstrates these relationships. This type of pattern is believed to reflect magma generation involving hydrous fluids in the mantle source overlying the downgoing lithospheric slab (Best, 2003). Both the REE diagram and spider diagram must be normalized in order to smooth out ups and downs due to the greater abundances of even atomic numbers over odd atomic numbers (Oddo-Harkins rule). Referencing primitive materials also makes measurements easier to judge than absolute concentrations. The REE plot (Fig. 15) is normalized using element concentrations in average chondritic meteorites, while the spider diagram (Fig. 16) is normalized using average primitive mantle.

The Dayingshan rock sample is metaluminous, with an alumina saturation index (ASI) molecular ratio ($Al_2O_3/(CaO+K_2O+Na_2O)$) of 0.91 and $Al_2O_3/(K_2O+Na_2O)$ of 1.63. Metaluminous rocks are defined as having molecular Al_2O_3 greater than (K_2O+Na_2O) but less than $(CaO+K_2O+Na_2O)$. Metaluminous samples are typically felsic, and the deficiency in alumina is accommodated in hornblende and biotite. A metaluminous composition, coupled with high Zr concentrations, would likely stabilize any entrained zircon xenocrysts if they were present (Zou et al., 2010).

Polished Zircon Core Ages

Zircon cores were measured by SIMS to attain the oldest ages of the minerals. Dayingshan zircons did not show well-developed growth-zoning, however they did provide enough surface area for SIMS analysis. Selected zircon cathodoluminescence images are shown in Figure 17. Twenty-two polished zircon cores were measured (Table 4), with 21 grains yielding an apparent U/Th isochron

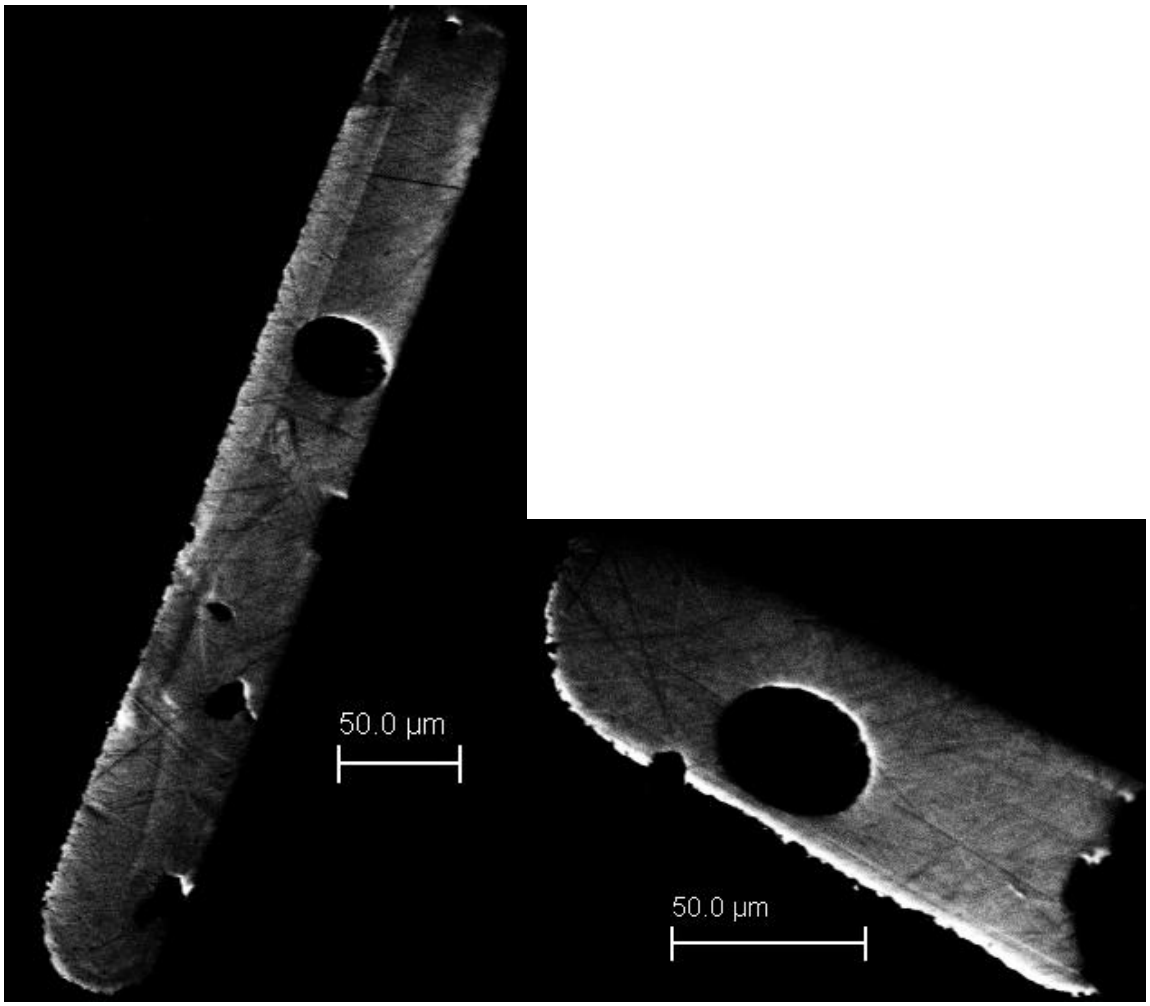

Fig. 17. Cathodoluminescence images of sample Day-int4 and Day-int1 with SIMS crater spots. Growth zoning is not well-developed in these zircons.

Table 4

U/Th isotope data, concentrations, and ages for Dayingshan zircon cores as measured by SIMS. Ages were calculated using Isoplot (Ludwig, 2003). 1s is the standard error and is a measurement of uncertainty.

Sample	($^{238}U/^{232}Th$)	1s	($^{230}Th/^{232}Th$)	1s	U (ppm)	Th (ppm)	Th/U	$D_{Th/U}$	Age (ka)	+ (ka)	- (ka)
Day-int1	1.326	0.025	2.384	0.046	2644	1929	0.73	0.07	83.6	3.8	-3.7
Day-int2	0.597	0.017	1.214	0.045	529	858	1.62	0.15	91.6	9.2	-8.5
Day-int3	0.543	0.011	0.93	0.044	395	704	1.78	0.17	62.2	6.6	-6.3
Day-int4	0.501	0.012	1.054	0.046	430	831	1.93	0.18	94.2	10.9	-9.9
Day-int5	0.491	0.023	0.943	0.046	369	727	1.97	0.19	76.1	10.9	-9.9
Day-int6	0.446	0.008	0.979	0.032	681	1479	2.17	0.21	100.1	9.3	-8.6
Day-int7	0.245	0.005	0.599	0.030	353	1396	3.95	0.37	98.6	19.8	-16.7
Day-int8	0.324	0.006	0.72	0.034	397	1186	2.99	0.28	89.5	13.1	-11.7
Day-int9	0.293	0.005	0.761	0.024	769	2543	3.31	0.31	136.4	18.1	-15.5
Day-int10	0.542	0.013	1.131	0.054	499	891	1.79	0.17	94.6	11.5	-10.4
Day-int11	0.557	0.012	1.039	0.032	753	1309	1.74	0.16	74.8	5.7	-5.4
Day-int12	0.65	0.008	1.242	0.026	1377	2051	1.49	0.14	82.4	4.1	-3.9
Day-int13	0.604	0.014	1.107	0.041	509	815	1.60	0.15	74.2	6.6	-6.2
Day-int14	0.583	0.011	1.314	0.174	496	823	1.66	0.16	114.6	43.5	-31.0
Day-int15	0.53	0.01	1.054	0.045	395	721	1.83	0.17	84.6	8.7	-8.1
Day-int16	1.36	0.036	3.736	0.174	231	165	0.71	0.07	216.3	49.6	-34.0
Day-int17	0.479	0.011	0.966	0.034	510	1030	2.02	0.19	84.3	7.8	-7.3
Day-int18	1.354	0.029	2.025	0.142	266	190	0.72	0.07	61.7	7.5	-7.0
Day-int19	0.42	0.006	0.924	0.034	507	1168	2.30	0.22	98.0	9.9	-9.0
Day-int20	0.575	0.009	1.064	0.026	1233	2074	1.68	0.16	74.4	4.2	-4.1
Day-int21	0.512	0.014	1.03	0.040	700	1325	1.89	0.18	85.8	9.0	-8.3
Day-int22	0.418	0.006	0.772	0.033	405	939	2.32	0.22	64.7	6.9	-6.5

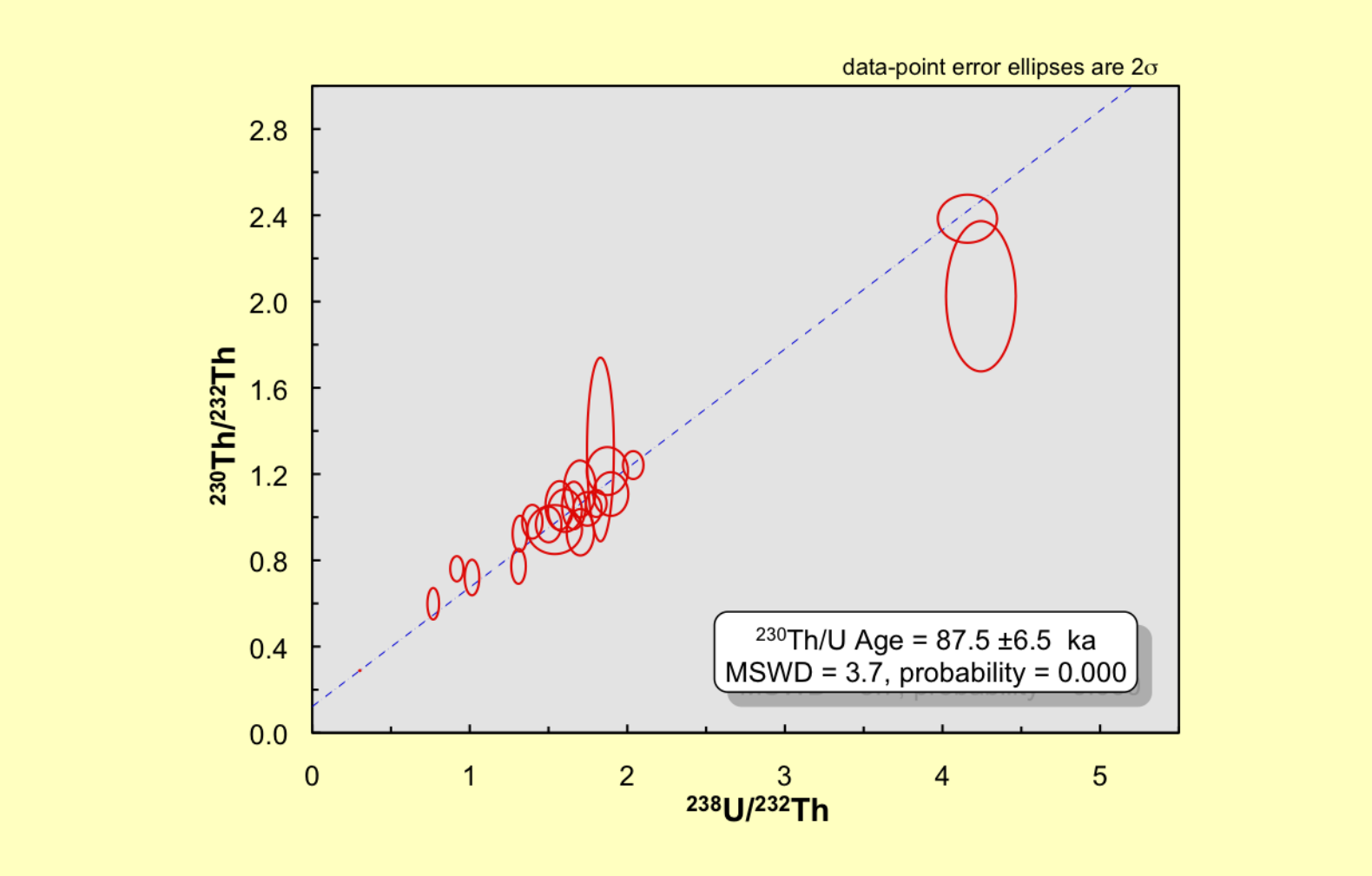

Fig. 18. U/Th isochron plot for zircon cores from Dayingshan. Chart was constructed and ages were determined using Isoplot (Ludwig, 2003).

age of 87.5 ± 6.5 ka (Fig. 18), with a mean square of weighted deviates (MSWD) of 3.7. This data is similar to a calculated age of 83.5 ± 9 ka for interiors of Maanshan zircons (Zou et al., 2010). Sample Day-int16 was disregarded due to an inherently low U ppm. The MSWD is essentially an expression of scatter, and is used to infer how many zircon populations are present. Generally, an MSWD of <2.5 is considered to define an isochron (Brooks et al., 1972). While an MSWD of 3.7 is higher than this cutoff, a mixture modeling chart, based on the probability density function, of U/Th ages of Dayingshan zircon interiors (Fig. 19) shows a single mode of zircons. This is interpreted as representing a likely single population of zircons.

Unpolished Zircon Rim Ages

Because the outer rims of Dayingshan zircons were smaller than the typical beam spot of 25 μm, shallow (< 3 μm) depth profiling analysis was used. Depth profiling allows for specific targeting of the surface of natural zircon crystal faces. U/Th ages of 17 unpolished zircon grains were measured (Table 5). One of these zircon measurements was disregarded due to high background readings. The U/Th measured ages of the zircon rims is 58 ± 13 ka, with a MSWD of 1.8 (Fig. 20). This age data is similar to the calculated age of 53.6 ± 5 ka by Zou et al. (2010) of unpolished zircons from Maanshan volcano.

Comparison of Core and Rim Ages

Calculated core ages (87.5 ± 6.5 ka) are significantly older than the rim ages (58 ± 13 ka), representing at least two different magmatic events. This older

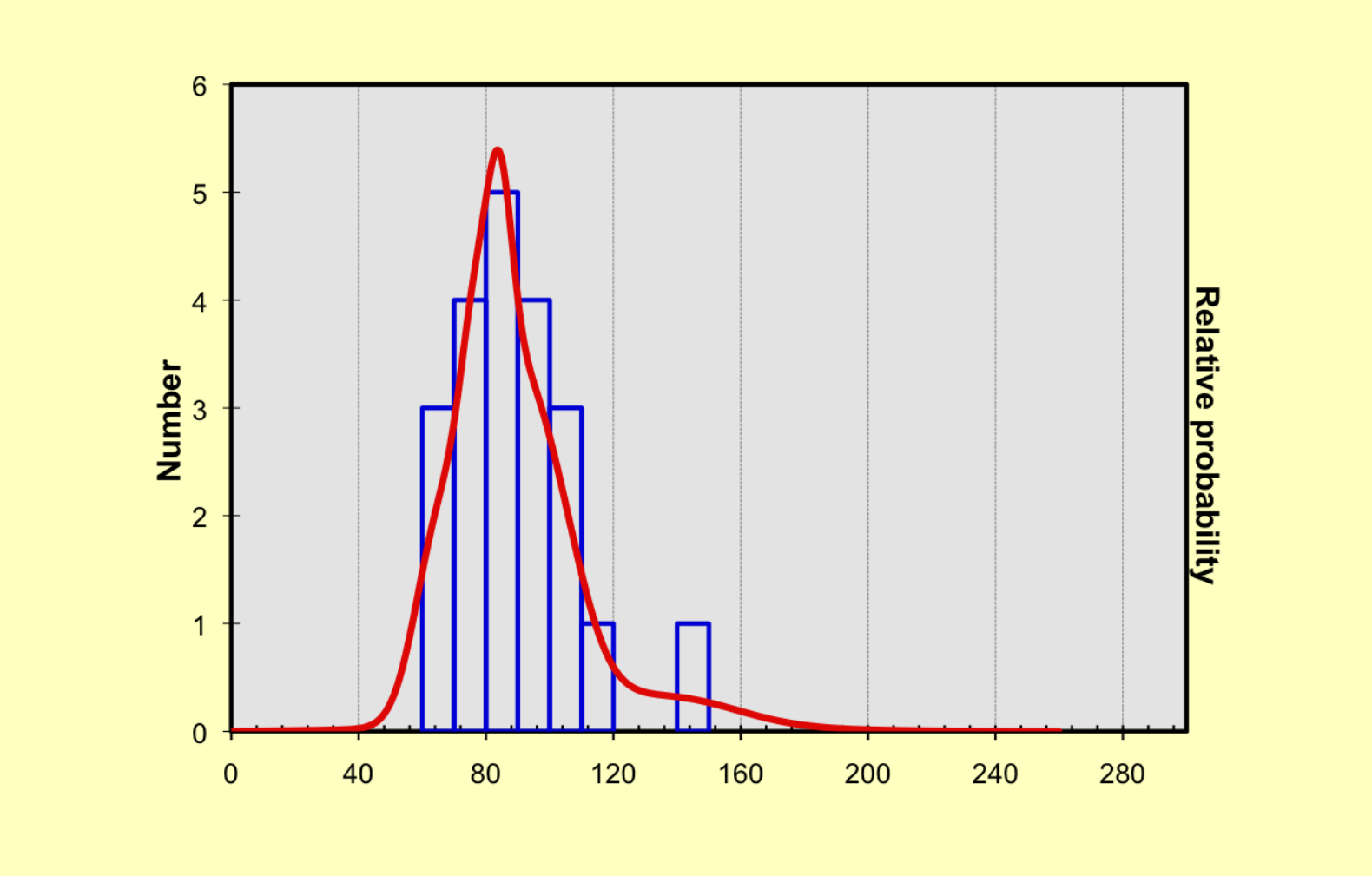

Fig. 19. Mixture modeling plot of zircon core ages from Dayingshan produced using the probability density function from Isoplot (Ludwig, 2003).

Table 5
U/Th isotope data, concentrations and ages for Dayingshan zircon rims as measured by SIMS. Ages were calculate using Isoplot (Ludwig, 2003). 1s is the standard error and is a measurement of uncertainty.

Zircon Sample	$(^{238}U/^{232}Th)$	1s	$(^{230}Th/^{232}Th)$	1s	U (ppm)	Th (ppm)	Th/U	$D_{Th/U}$	Age (ka)	+ (ka)	- (ka)
Day-rim1	1.420	0.020	3.360	0.210	988	674	0.68	0.06	144.8	23.6	-19.4
Day-rim2	0.502	0.015	1.045	0.036	924	1781	1.93	0.18	94.2	9.4	-8.7
Day-rim3	0.595	0.012	1.225	0.058	371	604	1.63	0.15	96.1	11.0	-10.0
Day-rim4	0.768	0.013	1.617	0.117	415	522	1.26	0.12	105.6	17.5	-15.1
Day-rim5	1.008	0.028	1.593	0.054	732	703	0.96	0.09	65.2	4.7	-4.5
Day-rim6	0.538	0.008	1.075	0.035	622	1119	1.80	0.17	87.9	6.8	-6.4
Day-rim7	0.280	0.007	0.759	0.053	266	921	3.46	0.33	163.6	59.5	-38.3
Day-rim8	0.566	0.024	1.135	0.054	450	770	1.71	0.16	89.8	12.0	-10.8
Day-rim9	0.449	0.008	1.017	0.033	660	1422	2.15	0.20	110.9	10.4	-9.5
Day-rim10	0.757	0.020	1.364	0.064	545	697	1.28	0.12	77.7	7.9	-7.4
Day-rim11	0.887	0.018	1.731	0.070	541	590	1.09	0.10	92.9	8.2	-7.6
Day-rim12	0.699	0.010	1.374	0.038	981	1358	1.38	0.13	90.4	5.7	-5.4
Day-rim13	0.829	0.015	1.392	0.044	1050	1226	1.17	0.11	69.6	4.5	-4.3
Day-rim14	0.656	0.010	1.349	0.062	591	873	1.48	0.14	97.9	10.3	-9.4
Day-rim15	0.573	0.017	1.192	0.062	484	817	1.69	0.16	97.4	13.0	-11.6
Day-rim16	0.851	0.016	1.837	0.095	328	373	1.14	0.11	112.9	13.7	-12.2
Day-rim17	0.458	0.008	0.975	0.033	908	1921	2.11	0.20	96.5	8.7	-8.1

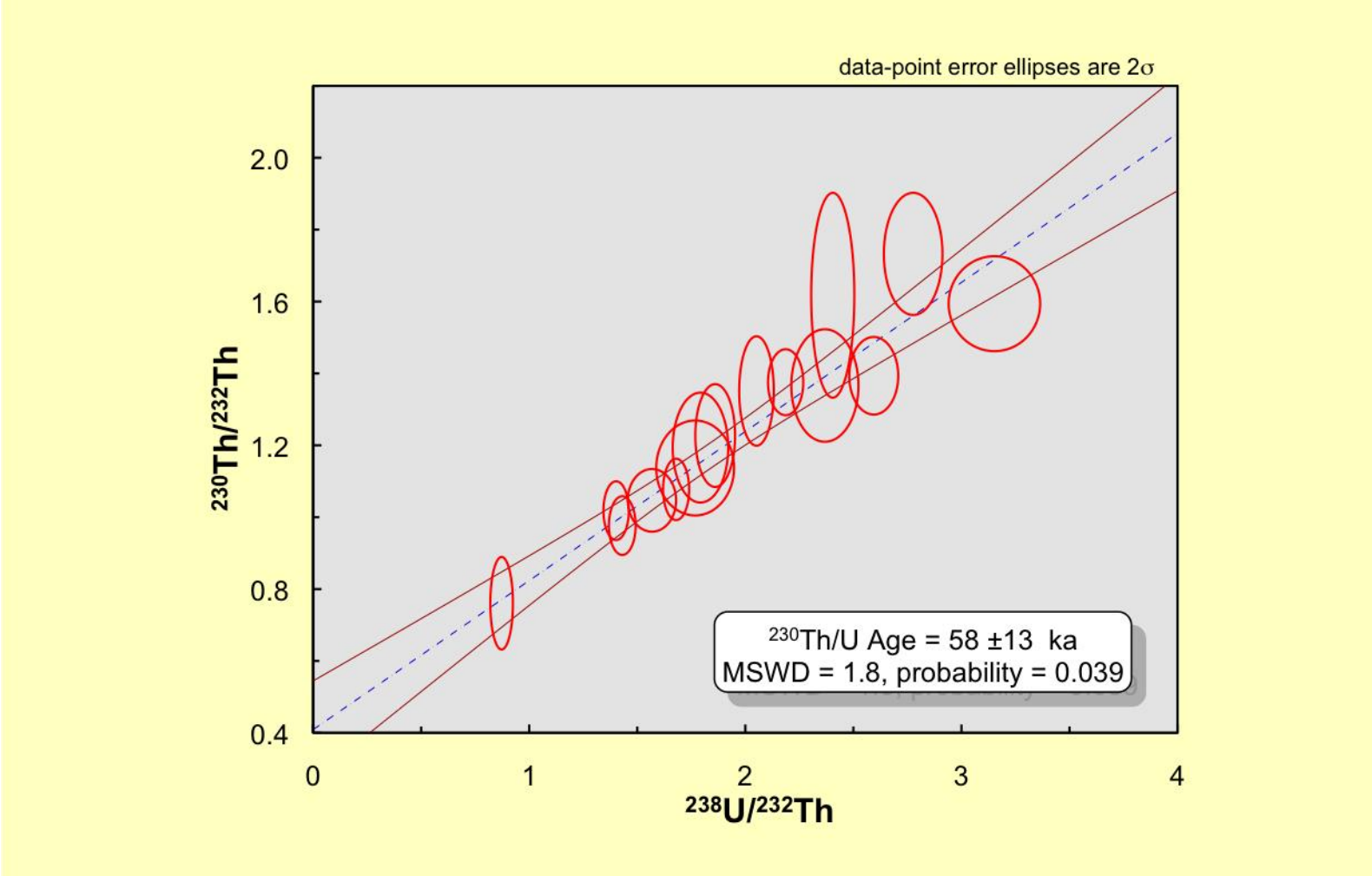

Fig. 20. U/Th isochron plot for zircon rims from Dayingshan using shallow depth profiling. Chart was constructed and ages were determined using Isoplot (Ludwig, 2003).

population is not old enough to be incorporated xenocrysts from basement rock, however it may represent zircons that have been remobilized from an earlier magmatic episode (Zou et al., 2010). These zircons could be considered antecrysts, in that they grew from predecessor magmas left over in the magma chamber. This could be tested with U/Th dating of rocks from previous Quaternary eruptive events from Dayingshan.

Zircon Saturation

Whether the melt was saturated with respect to zircon is important when trying to interpret possible zircon inheritance from country rock. Zircon saturation is a function of both magma composition and temperature, and is defined by the equation:

$$\ln D_{Zr}^{zircon/melt} = (-3.80 - [0.85(M-1)]) + \frac{12900}{T}$$

where $D_{Zr}^{zircon/melt}$ is the concentration ratio of Zr in zircon to Zr in the melt, M represents the melt composition ((Na+K+2Ca)/(Al×Si)), and T is the temperature in Kelvin. This study uses zircon saturation as a means to deduce zircon inheritance in the system. According to major element compositions in Dayingshan YTC9724-5, M = 1.87. An estimated temperature of 750°C is used based on Ti-in-zircon geothermometry from Maanshan (Zou et al., 2010). Using these two variables, the Zr concentration needed to saturate the melt is 156 ppm. Because whole-rock analysis yielded a Zr concentration of 303 ppm, and only 156 ppm is needed to

saturate the melt, we can infer that the melt was saturated in Zr. Under these saturated conditions, any inherited zircons from country rock would remain stable in the melt. This knowledge, along with the fact that no zircons as old as the country rock have been found, provides evidence that there is no contamination from country rock.

DISCUSSION

Magma Chamber Storage Time

Storage of magma in magma chambers is often poorly understood because it is difficult to isotopically date materials recording the duration. A determination of magma storage time in the Tengchong volcanic field is important for several reasons. A better understanding of magma chamber processes could provide valuable insights into the ascent and storage of magma, especially in this unique volcanic environment. This information could prove valuable to the many people who live in close proximity to the active volcanoes. In large part, industry and tourism attract people into areas within active geothermal fields (Wei et al., 2003). Figure 21 is a map showing the distribution of some of the major cities and villages in the Tengchong volcanic field. In addition to industry and tourism, fertile volcanic soil for growing crops is another factor leading to increased population in this area.

Basement rocks to the Tengchong volcanoes are mostly granites with ages ~5.5 Ma (Ji, 1998). Other country rocks in the area include Paleozoic gneisses and Carboniferous sandstones. Since all these rocks are significantly older than measured Dayingshan zircon ages (58 and 87.5 ka), and because inherited zircons would have been stable in the melt if they were present, it is safe to assume that there are no inherited zircons from country rock. Therefore, the zircons present must have formed in the magma chamber prior to eruption. We can infer magma

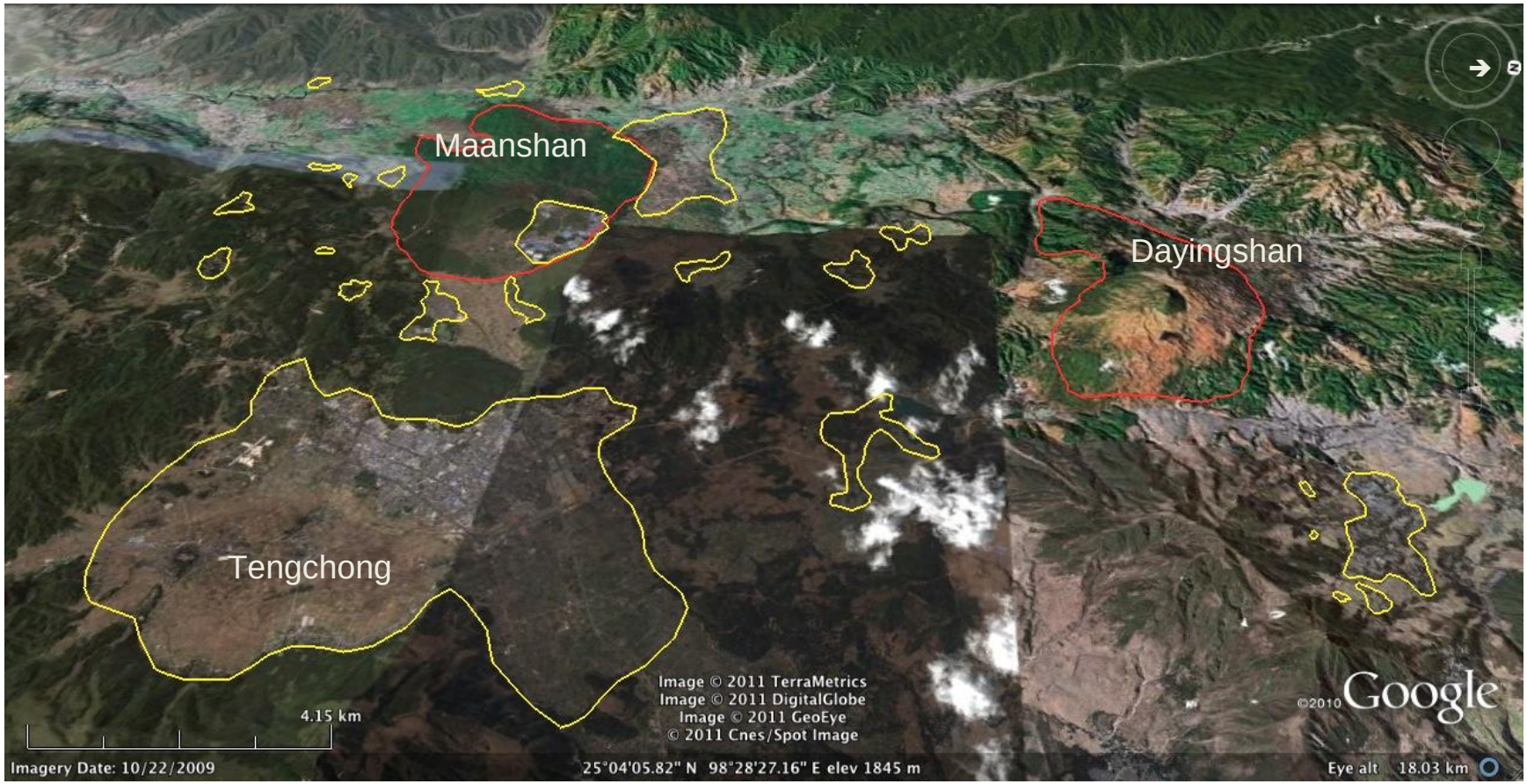

Fig. 21. Satellite image of the southern portion of the Tengchong volcanic field showing the distribution of some of the major cities and villages in the region. Maanshan and Dayingshan are outlined in red. Major cities and villages, including Tengchong (population 620,000), are outlined in yellow. Map produced using Google Earth.

chamber storage time by subtracting the volcanic eruption event that yielded the basaltic andesites from the calculated zircon ages. Using an eruption age of ~10 ka (Zou et al., 2010), a magma chamber storage time of 48 ka is determined for zircon rims and 77.5 ka for zircon cores.

Th/U Ratios

Dayingshan zircons have higher than average Th/U ratios for igneous zircons. An average Th/U ratio for most igneous zircons is ~0.5, and typically ranges from 0.2 - 0.9 (Bindeman et al., 2006). Unusually high Th/U ratios are often indicative of a continental crust component in the melt. Dayingshan cores have an averageTh/U ratio of 1.92, and range from 0.71 – 3.95. Dayingshan rims have an average Th/U ratio of 1.58, and range from 0.68 – 3.46. Though the variation in Th/U ratios is high, zircon rims yielded only slightly lower ratios than zircon cores. A rimward decrease in Th/U ratios is indicative of fractionation during zircon growth (Zou et al., 2010). Despite the slight difference in Th/U ratios, the similarity between core and rim ratios suggests the crystals share a closed-system evolution, implying that contamination in the magma system since the zircon core formation is minimal (Zou et al., 2010).

In order to determine if the high Th/U ratios in the Dayingshan zircons are a result of high Th/U ratios in the original melt, the mineral/melt partitioning coefficients ($D_{Th/U}$) for the concentrations of Th and U must be determined. $D_{Th/U}$ is the ratio of concentration of U and Th in a crystallizing zircon to concentration of these elements in the melt. $D_{Th/U}$ is calculated by the following equation:

$$D_{Th/U} = \frac{D_{Th}}{D_U} = \frac{Th_{zircon}/Th_{melt}}{U_{zircon}/U_{melt}} = \frac{Th_{zircon}/U_{zircon}}{Th_{melt}/U_{melt}}$$

Using this equation, and a Th/U melt ratio of 10.6 determined from the isotope dilution method at National Taiwan University, the average $D_{Th/U}$ is 0.18 ± 0.07 for zircon cores and 0.15 ± 0.06 for zircon interiors. Uncertainty for calculated $D_{Th/U}$ is large due to the large spread in Th/U ratios, however, $D_{Th/U}$ is fairly constant for most igneous rock compositions. These $D_{Th/U}$ measurements are similar to an average $D_{Th/U}$ of 0.26 ± 0.16 for zircons from intermediate rocks (55-65 wt% SiO_2), in spite of their high Th/U ratios that typically suggest a more felsic composition. Because of this, it is safe to assume that the high Th/U ratios in Dayingshan zircons were inherited from a high Th/U melt.

Comparison of Dayingshan and Maanshan Data

Isotopic and trace element data accumulated from Dayingshan reinforces data from an earlier study of Maanshan by Zou et al. (2010). Maanshan is another recently active volcano in the Tengchong volcanic field, and lies ~13 km to the south of Dayingshan (Fig. 2). Similar SiO_2, K_2O and Na_2O contents (58.46, 3.40 and 3.79 wt% in Maanshan; 62.24, 4.05 and 3.29 wt% in Dayingshan) indicate similar rock composition, and provide evidence for differentiation of the lavas. Zr concentrations are also high in Maanshan (260 ppm) and Dayingshan (303 ppm). Because high SiO_2 contents provide favorable conditions for zircon crystals to form, and Zr melt concentrations from both volcanoes are high, rocks contain abundant

amounts of zircon crystals. Lavas from both volcanoes also have metaluminous compositions, with Maanshan (1.67) rocks showing a slightly higher $Al_2O_3/(K_2O+Na_2O)$ value than Dayingshan (1.63).

Measured Maanshan Th/U ratios ranged from 0.65 to 5.1 for zircon interiors and 0.32 to 2.44 from zircon rims, which are unusually high for igneous zircons. These high ratios were also measured from Dayingshan (0.71 to 3.95 for zircon interiors and 0.68 to 3.46 for zircon rims). Because higher Th/U ratios reflect a more enriched source, this is a strong indication for a melt with a crustal component. One significant difference between Th/U measurements is that Maanshan zircon cores have two (young and old) populations while Dayingshan zircon cores have only one (old) age population. The apparent lack of young zircon cores at Dayingshan might be due to limited sampling.

Age calculations also seem to correspond between the two volcanoes. Analysis of zircons from Maanshan recorded a bimodal population for zircon interiors, with calculated ages of 55 ± 7 ka for the younger population and 91 ± 6 ka for the older population. Zircon rims recorded an age of 53.6 ± 5 ka. Dayingshan zircon interior measurements yielded a unimodal age of 87.5 ± 6 ka, while zircon rim measurements yielded an age of 58 ± 13 ka. The older age population from Maanshan zircon interiors is consistent with the age of Dayingshan zircon interiors, and Maanshan zircon rim ages are consistent with Dayingshan zircon rim ages. This consistency further reaffirms the validity of the age data, and provides greater confidence in the capabilities of SIMS. Better constraints on population ages could

be reinforced by future studies of Heikongshan volcano (Fig. 2), which lays ~10 km north of Dayingshan.

Assessment of Magma Origins

Trace element data, along with Nd and Sr isotopic data from several studies (Zhu et al., 1983; Wang, F. et al., 2006; Zou et al., 2010), display enriched mantle characteristics. Enriched signatures are indicative of a crustal element in the melt that could be introduced into the system in several different ways. One way to potentially introduce a continental element is from continental contamination through assimilation of country rock. This is an unlikely source due to the fact that none of the 60+ zircons dated between this study and Zou et al. (2010) have recorded ages as old as the country rocks in Tengchong. Xenocrysts could not have re-dissolved into the magma because a melt saturated in Zr (303 ppm) and a metaluminous composition would stabilize any incorporated zircon xenocrysts.

With crustal contamination ruled out, the U-Th data in this study indicates continental subduction as a likely origin for the volcanism in the Tengchong volcanic field. While it is clear that Indian plate subduction does not reach as far as the field (Wang & Long, 1998; Lei et al., 2009), it is likely that stagnant slab from prior subduction is responsible for continental crust signatures in the magma. This conclusion is further reinforced by the presence of high-velocity anomalies in the mantle transition zone (Lei et al., 2009).

Typically, rocks showing ^{238}U excesses indicate a continental subduction source because U is more easily mobilized in fluid, representing fluid fluxing in the

mantle. The dehydration of mantle previously metasomatized by subduction is a likely source for the ^{238}U excesses in some Tengchong volcanic field magmas (Wang, F. et al., 2006). Indeed, most samples from Maanshan volcano show ^{238}U excesses (Wang, F. et al., 2006; Zou et al., 2010).

The Dayingshan sample in this study measured slight ^{230}Th enrichment relative to ^{238}U, with ^{230}Th excesses of ~4.8%. ^{230}Th excesses in Dayingshan rocks have also been reported by Wang, F. et al. (2006). The presence of both ^{238}U excess and slight ^{230}Th excess lavas is commonly observed in continental arc volcanoes, even within a single volcano (e.g. Garrison et al., 2006). During decompressional melting, several factors may influence the ratio of ^{230}Th to ^{238}U, however only the bulk partition coefficients, and thus the source mineralogy, determine whether $^{230}Th/^{238}U$ is greater than or less than 1 (Zou et al., 2003). The range in U-Th disequilibrium at Maanshan and Dayingshan may be due to melting of a mantle with heterogeneous source mineralogy as a result of variable fluid addition and sediment contribution, which are to be expected in a continental arc setting.

CONCLUSIONS

Volcanism in the Tengchong volcanic field has been active since the late Tertiary, and has been punctuated by four major eruptive stages representing slightly different magmatic compositions. Varying major and trace element signatures, as well as structural and tectonic complexities in the formation of the region, have created questions regarding the formation and magmatic evolution of the volcanic field. Dayingshan is one of the three most recently active volcanoes in the field. Due to a relative abundance of zircon, rocks from the Tengchong volcanic field can be radiometrically dated using ^{238}U-^{230}Th dating methods. The spatial resolution, low background and high sensitivity capabilities of SIMS are required to date the zircons due to their relatively small sizes and low Th abundances in the Quaternary rocks.

The Dayingshan zircons indicate two age populations at 58 ± 13 ka and 87.5 ± 6.5 ka. The older population most likely represents zircon antecrysts that were formed in an earlier phase of magmatism, but remained in the magma chamber and remobilized in a second magmatic phase. The younger population represents phenocrystic growth in the most recent magma body. Using this age population, a magma chamber storage time of 48 ka is deduced by subtracting the most recent eruption age (~10 ka) from the zircon age.

Dayingshan whole-rock major and trace element analysis yielded high Zr concentrations and an overall calc-alkaline trend. Enrichment in LREE's and incompatible elements, and depletion in elements with high field strengths were measured, and are typical in subduction-related melts. The whole-rock chemistry points to a metaluminous signature, and measurements of zircon saturation indicate that the melt was saturated with respect to Zr. These factors indicate that there is no incorporation of zircon xenocrysts from the country rock. This conclusion is further reinforced by the fact that no zircon has yet been found in the Dayingshan lavas to date as old as the country rock. Trace element and isotopic data from this and other studies have found enriched mantle characteristics, indicating a crustal component in the melt. This has lead to the conclusion that the magma likely originated from fluid fluxing off of a stagnant slab from a prior subduction event.

Major and trace element analysis and calculated ages for zircons from Dayingshan and Maanshan (Zou et al., 2010) have yielded similar results. The slight range in whole-rock U-Th disequilibrium at Maanshan and Dayingshan may be due to melting of a mantle with heterogenous source mineralogy as result of variable fluid addition and sediment contribution, which is to be expected in a continental arc setting.

REFERENCES

Bai, D., Meju, M.A., and Liao, Z., 2001. Magnetotelluric images of deep crustal structure of the Rehai geothermal field near Tengchong, southern China. Geophysical Journal International 147, 677-687.

Best, M.G., 2003. *Igneous and Metamorphic Petrology*, 2nd ed.: Blackwell Publishing, Massachusetts, 729 p.

Berg, R., 2008. *Radioactive and Nuclear Decay*, Retrieved from http://www.physics.umd.edu/lecdem/honr228q/notes/notesl.htm

Bindeman, I.N., Schmitt, A.K., Valley, J.W., 2006. U-Pb zircon geochronology of silicic tuffs from the Timber Mountain/Oasis Valley caldera complex, Nevada: rapid generation of large volume magmas by shallow-level remelting. Contributions to Mineralogy and Petrology 152, 649-665.

Brooks, C., Hart, S.R., Wendt, I., 1972. Realistic use of two-error regression treatments as applied to rubidium-strontium data. Review of Geophysics and Space Physics 10, 551-577.

Condomines, M., 1997. Dating recent volcanic rocks through ^{230}Th-^{238}U disequilibrium in accessory minerals; example of the Puy de Dome (French Massif Central). Geology 25, 375-378.

Cong, B.L., Chen, Q.Y., Zhang, R.Y., Wu, G.Y., and Xu, P., 1994. Genesis of Tengchong volcanics, China. Science in China Series B, 24, 441-448.

Evans Analytical Group LLC, 2010. *SIMS Theory: Ion Beam Sputtering*, Retrieved from http://www.eaglabs.com/training/tutorials/sims_theory_tutorial/ionsput.php

Fan, P.F., 1978. Outline of tectonic evolution of southwestern China. Tectonophysics 45, 261-267.

Finch, R.J., and Hanchar, J.M., 2003. Structure and chemistry of zircon and zircon-group minerals. *In* Zircon, Reviews in Mineralogy & Geochemistry 53 (J.M. Hanchar, and P.W.O. Hoskin, eds.). The Mineralogical Society of America, Washington, 1-25.

Garrison, J., Davidson, J., Reid, M., and Turner, S., 2006. Source versus differentiation controls on U-series disequilibria: Insights from Cotopaxi Volcano, Ecuador. Earth and Planetary Science Letters 244, 548-565.

Heaman, L.M., Bowins, R., and Crocket, J., 1990. The chemical composition of igneous zircon suites: implications for geochemical tracer studies. Geochim Cosmochim Acta 54, 1597-1607.

Hoskin, P.W.O., and Ireland, T.R., 2000. Rare earth element chemistry of zircon and its use as a provenance indicator. Geology 28, 627-630.

Hoskin, P.W.O., and Schaltegger, U., 2003. The composition of zircon and igneous and metamorphic petrogenesis. *In* Zircon, Reviews in Mineralogy & Geochemistry 53 (J.M. Hanchar, and P.W.O. Hoskin, eds.). The Mineralogical Society of America, Washington, 27-62.

Ireland, T.R., and Williams, I.S., 2003. Considerations of zircon geochronology by SIMS. *In* Zircon, Reviews in Mineralogy & Geochemistry 53 (J.M. Hanchar, and P.W.O. Hoskin, eds.). The Mineralogical Society of America, Washington, 215-241.

Irvine, T.N. and Baragar, W.R.A., 1971. A guide to the chemical classification of the common volcanic rocks. Canadian Journal of Earth Sciences 8, 523-548.

Ji, J.Q., 1998. Petrology and Cenozoic lithosphere tectonic evolution of Tengchong-Yingjiang-Nabang area, west Yunnan, south-west China. PhD dissertation, Chinese Academy of Sciences, 1-88.

Košler, J., and Sylvester, P.J., 2003. Present trends and the future of zircon in geochronology: Laser Ablation ICPMS, *In* Zircon, Reviews in Mineralogy & Geochemistry 53 (J.M. Hanchar, and P.W.O. Hoskin, eds.). The Mineralogical Society of America, Washington, 243-275.

LaTourrette, T.Z., Kennedy, A.K., and Wasserburg, G.J., 1993. U-Th fractionation by garnet- Evidence for a deep source and rapid rise by oceanic basalts, Science 261, 739-742.

Li, D.M., Li, Q., Chen, W.J., 2000. Volcanic activity of Tengchong since the Pliocene. Acta Petroligica Sinica 16, 362-370.

Lei, J.S., Zhao, D.P., Su, Y.J., 2009. Insight into the origin of the Tengchong intraplate volcano and seismotectonics in southwest China from local and teleseismic data. Journal of Geophysical Research 114, B05302. doi: 10.1029/2008JB005881.

Ludwig, K.R., 2003. User's Manual for ISOPLOT 3.00: A geochronological toolkit for Microsoft Excel. Berkeley Geochronology Center Special Publication No. 4, Berkely, 70 p.

Mu, Z.G., Tong, W., Curtis, G.H., 1987. Timing of Tengchong volcanic activities and related magmatic source. Acta Geophysica 30, 261-270.

Perkins, D., 2002. *Mineralogy*, 2nd ed.: Prentice Hall, New Jersey, 483 p.

Reid, M.R., Coath, C.D., Harrison, T.M., and McKeegan, K.D., 1997. Prolonged residence times for the youngest rhyolites associated with Long Valley Caldera: 230Th-238U ion microprobe dating of young zircons. Earth and Planetary Science Letters 150, 27-29.

Schmitt, K.A., 2009, Chapter 5: Quaternary Geochronology by SIMS. Mineralogical Association of Canada Short Course 41, Toronto, 109-131.

Simon, J.I., Renne, P.R., and Mundil, R., 2008. Implications of pre-eruptive magmatic histories of zircons for U-Pb geochronology of silicic extrusions. Earth and Planetary Science Letters 266, 182-194.

Stern, R.A., 2009, Chapter 1: An Introduction to Secondary Ion Mass Spectrometry (SIMS) in Geology. Mineralogical Association of Canada Short Course 41, Toronto, 1-18.

Tapponnier, P., Peltzer, G., Le Dain, A.Y., Armijo, R., and Cobbold, P., 1982. Propagating extrusion tectonics in Asia: New insights from simple experiments with plasticine. Geology 10, 611-616.

"UCLA SIMS Home Page." http://sims.ess.ucla.edu/index.php. Accessed January 20, 2011.

Wang, S.J., and Long, X.F., 1998. Distribution and characteristics of seismic mechanism and tectonic stress field in Tengchong volcanic area and its adjacent regions. China Seismic Research 21, 349-357.

Wang, F., Peng, Z.C., Zhu, R.X., He, H.Y., and Yang, L.K., 2006. Petrogenesis and magma residence time of lavas from Tengchong volcanic field (China): Evidence from U series disequilibria and $^{40}Ar/^{39}Ar$ dating. Geochemistry, Geophysics, Geosystems 7, Q01002 10.1029.

Wang, Y., Zhang, X., Jiang, C., Wei, H., and Wan, J., 2006. Tectonic controls on the late Miocene-Holocene volcanic eruptions of the Tengchong volcanic field along the southeastern margin of the Tibetan plateau. Journal of Asian Earth Sciences 30, 375-389.

Wei, H., Sparks, R.S.J., Liu, R., Fan, Q., Wang, Y., Hong, H., Zhang, H., Chen, H., Jiang, C., Dong, J., Zheng, Y., & Pan, Y., 2002. Three active volcanoes in China and their hazards. Journal of Asian Earth Sciences 21, 515-526.

Wilde, S.A., Valley, J.W., Peck, W.H., Graham, C.M., 2001. Evidence from detrital zircons for the existence of continental crust and oceans on the Earth 4.4 Gyr ago. Nature 409, 175-178.

Zhao, Y.W., and Fan, Q.C., 2010. Magma origin and evolution of Maanshan volcano, Dayingshan volcano and Heikongshan volcano in Tengchong area. Acta Petrologica Sinica 26, 1133-1140.

Zhu, B.Q., Mao, C.X., Lugmair, G.W., and Macdougall, J.D., 1983. Isotopic and geochemical evidence for the origin of Plio-Pleistocene volcanic rocks near the Indo-Eurasian collisional margin at Tengchong, China. Earth and Planetary Science Letters 65, 263-275.

Zou, H.B., 2009. *Quantitative Geochemistry*: Imperial College Press, London, 291 p.

Zou, H.B., 2010. Dayingshan whole-rock analysis data. Unpublished raw data.

Zou, H.B., and Fan, Q.C., 2010. U-Th isotopes in Hainan basalts: Implications for sub-asthenospheric origin of EM2 mantle endmember and the dynamics of melting beneath Hainan Island. Lithos 116, 145-152.

Zou, H.B., Fan, Q.C., Schmitt, A.K., & Sui, J.L., 2009. U-Th constraints for fluid induced melting beneath the SE Tibetan Plateau (Maanshan volcano, Tengchong). Poster presented at: Fall 2009 American Geophysical Union Meeting, Dec 14-18; San Francisco, CA.

Zou, H.B., Fan, Q.C., Schmitt, A.K., and Sui, J., 2010. U-Th dating of zircons from Holocene potassic andesites (Maanshan volcano, Tengchong, SE Tibetan Plateau) by depth profiling: Time scales and nature of magma storage. Lithos 118, 202-210.